

Model-Based Epistemic Variance of Values for Risk-Aware Policy Optimization

Carlos E. Luis, Alessandro G. Bottero, Julia Vinogradska,
Felix Berkenkamp, and Jan Peters, *Fellow, IEEE*

Abstract—We consider the problem of quantifying uncertainty over expected cumulative rewards in model-based reinforcement learning. In particular, we focus on characterizing the *variance* over values induced by a distribution over MDPs. Previous work upper bounds the posterior variance over values by solving a so-called uncertainty Bellman equation (UBE), but the over-approximation may result in inefficient exploration. We propose a new UBE whose solution converges to the true posterior variance over values and leads to lower regret in tabular exploration problems. We identify challenges to apply the UBE theory beyond tabular problems and propose a suitable approximation. Based on this approximation, we introduce a general-purpose policy optimization algorithm, Q -Uncertainty Soft Actor-Critic (QU-SAC), that can be applied for either risk-seeking or risk-averse policy optimization with minimal changes. Experiments in both online and offline RL demonstrate improved performance compared to other uncertainty estimation methods.

Index Terms—Model-Based Reinforcement Learning, Bayesian Reinforcement Learning, Uncertainty Quantification.



1 INTRODUCTION

THE goal of reinforcement learning (RL) agents is to maximize the expected return via interactions with an *a priori* unknown environment [1]. In model-based RL (MBRL), the agent learns a statistical model of the environment, which can then be used for efficient exploration [2], [3], [4]. The performance of deep MBRL algorithms was historically lower than that of model-free methods, but the gap has been closing in recent years [5]. Key to these improvements are models that quantify epistemic and aleatoric uncertainty [6], [7] and algorithms that leverage model uncertainty to optimize the policy [8]. Still, a core challenge in MBRL is to quantify the uncertainty in long-term performance predictions of a policy given a probabilistic model of the dynamics [9]. Quantification of uncertainty around the policy’s value enables risk-awareness, i.e., reasoning about the long-term risk of rolling out a policy, which has shown promising results for both risk-seeking [9], [10] and risk-averse [11], [12] policy optimization.

We adopt a Bayesian perspective on RL to characterize uncertainty in the decision process via a posterior distribution. This distributional perspective of the RL environment induces distributions over functions of interest for solving the RL problem, e.g., the *expected return* of a policy, also known as the value function. Our perspective differs from *distributional* RL [13], whose main object of study is the distribution of the *return* induced by the inherent stochasticity of the MDP and the policy. As such, distributional RL models *aleatoric*

uncertainty, whereas Bayesian RL focuses on the *epistemic* uncertainty arising from finite data of the underlying MDP. Recent work combines Bayesian and distributional RL for uncertainty-aware optimization of policies [14], [15].

We focus on model-based Bayesian RL, where the value distribution is induced by a posterior over MDPs. In particular, in this paper we analyze the *variance* of such a distribution of values and design algorithms to estimate it. [16] estimates uncertainty in value functions using statistical uncertainty propagation, with the caveat of assuming the value distribution is Gaussian. Previous results by [17], [11] establish upper-bounds on the posterior variance of the values by solving a so-called uncertainty Bellman equation (UBE), without assumptions on the value distribution.

Our contribution. Based on the UBE framework, we first present a result that closes the theoretical gap in previous upper-bounds. Our epistemic variance estimate shows improved regret when used as a signal for exploration in tabular problems. Second, we identify challenges in applying the UBE theory to practical problems and propose suitable approximations. The result is a general-purpose algorithm called Q -Uncertainty Soft Actor-Critic (QU-SAC) that can be applied for either risk-seeking or risk-averse policy optimization with minimal changes. We evaluate QU-SAC in exploration tasks from the DeepMind Control (DMC) suite [18] as well as offline RL tasks from the D4RL benchmark [19]. The results presented are an extension of those in [20]. We introduce a new proxy uncertainty reward that addresses previous challenges under function approximation and substantially extend the empirical evaluation of the proposed algorithm.

1.1 Related work

Model-free Bayesian RL. Model-free approaches to Bayesian RL directly model the distribution over values, e.g., with

- C. E. Luis, A. G. Bottero, J. Vinogradska and F. Berkenkamp are with Bosch Corporate Research, Renningen, Germany.
E-mail: {carlorenrique.luisgoncalves, alessandrogiacomo.bottero, julia.vinogradska, felix.berkenkamp}@bosch.com
- J. Peters is with Intelligent Autonomous Systems Group, Technical University Darmstadt, Darmstadt, Germany, and also with the German Research Center for Artificial Intelligence (DFKI), Darmstadt, Germany.
E-mail: jan.peters@tu-darmstadt.de.

normal-gamma priors [21], Gaussian Processes [22] or ensembles of neural networks [23]. [24] estimates value distributions using a backwards induction framework, while [25] propagates uncertainty using Wasserstein barycenters. [26] showed that, due to bootstrapping, model-free Bayesian methods infer a posterior over Bellman operators rather than values.

Model-based Bayesian RL. Model-based Bayesian RL maintains a posterior over plausible MDPs given the available data, which induces a distribution over values. The MDP uncertainty is typically represented in the one-step transition model as a by-product of model-learning. For instance, the well-known PILCO algorithm by [9] learns a Gaussian Process (GP) model of the transition dynamics and integrates over the model’s total uncertainty to obtain the expected values. In order to scale to high-dimensional continuous-control problems, [7] proposes PETS, which uses ensembles of probabilistic neural networks (NNs) to capture both aleatoric and epistemic uncertainty as first proposed by [27]. Both approaches propagate model uncertainty during policy evaluation and improve the policy via greedy exploitation over this model-generated noise. Dyna-style [2] actor-critic algorithms have been paired with model-based uncertainty estimates for improved performance in both online [28], [29] and offline [12], [30] RL.

Online RL - Optimism. To balance exploration and exploitation, provably-efficient RL algorithms based on *optimism in the face of the uncertainty* (OFU) [31], [4] rely on building upper-confidence (optimistic) estimates of the true values. These optimistic values correspond to a modified MDP where the rewards are enlarged by an uncertainty bonus, which encourages exploration. In practice, however, the aggregation of optimistic rewards may severely overestimate the true values, rendering the approach inefficient [32]. [17] shows that methods that approximate the variance of the values can result in much tighter upper-confidence bounds, while [33] demonstrates their use in complex continuous control problems. Similarly, [34] proposes a model-free ensemble-based approach to estimate the variance of values.

Offline RL - Pessimism. In offline RL, the policy is optimized solely from offline (static) data rather than from online interactions with the environment [35]. A primary challenge in this setting is known as *distribution shift*, which refers to the shift between the state-action distribution of the offline dataset and that of the learned policy. The main underlying issue with distribution shifts in offline RL relates to querying value functions out-of-distribution (OOD) with no opportunity to correct for generalization errors via online interactions (as in the typical RL setting). One prominent technique to deal with distribution shifts is known as *conservatism* or *pessimism*, where a pessimistic value function (typically a lower bound of the true values) is learned by regularizing OOD actions [36], [37]. Model-based approaches to pessimism can be sub-divided into uncertainty-free [38], [39] and uncertainty-based methods [12], [30], [40]. While uncertainty-free pessimism circumvents the need to explicitly estimate the uncertainty, the current state-of-the-art method CBOP [40] is uncertainty-based. Our QU-SAC algorithm falls into the uncertainty-based category and differentiates from prior work over which uncertainty it estimates: MOPO [12] uses the maximum aleatoric standard deviation of a

dynamics ensemble forward prediction, MOREL [30] is similar but uses the maximum pairwise difference of the mean predictions, CBOP [40] instead does approximate Bayesian inference directly on the Q -value predictions conditioned on empirical (bootstrapped) return estimates. Instead, QU-SAC learns a Bayesian estimate of the Q -values variance via approximately solving a UBE. To the best of our knowledge, this is the first time a UBE-based algorithm is used for offline RL.

Uncertainty in RL. Interest about the higher moments of the *return* of a policy dates back to the work of [41], showing these quantities obey a Bellman equation. Methods that leverage these statistics of the return are known as *distributional* RL [42], [13]. Instead, we focus specifically on estimating and using the *variance* of the *expected return* for policy optimization. A key difference between the two perspectives is the type of uncertainty they model: distributional RL models the *aleatoric* uncertainty about the returns, which originates from the aleatoric noise of the MDP transitions and the stochastic policy; our perspective studies the *epistemic* uncertainty about the value function, due to incomplete knowledge of the MDP. Provably efficient RL algorithms use this isolated epistemic uncertainty as a signal to balance exploring the environment and exploiting the current knowledge.

UBE-based RL. [17] proposes a UBE whose fixed-point solution converges to a guaranteed upper-bound on the posterior variance of the value function in the tabular RL setting. This approach was implemented in a model-free fashion using the DQN [43] architecture and showed performance improvements in Atari games. Follow-up work by [44] empirically shows that the upper-bound is loose and the resulting over-approximation of the variance impacts negatively the regret in tabular exploration problems. [11] proposes a modified UBE with a tighter upper-bound on the value function, which is then paired with proximal policy optimization (PPO) [45] in a conservative on-policy model-based approach to solve continuous-control tasks. Our QU-SAC algorithm integrates UBE-based uncertainty quantification into a model-based soft actor-critic (SAC) [46] architecture similar to [5], [47].

2 PROBLEM STATEMENT

We consider an agent that acts in an infinite-horizon MDP $\mathcal{M} = \{\mathcal{S}, \mathcal{A}, p, \rho, r, \gamma\}$ with finite state space $|\mathcal{S}| = S$, finite action space $|\mathcal{A}| = A$, unknown transition function $p : \mathcal{S} \times \mathcal{A} \rightarrow \Delta(S)$ that maps states and actions to the S -dimensional probability simplex, an initial state distribution $\rho : \mathcal{S} \rightarrow [0, 1]$, a known and bounded reward function $r : \mathcal{S} \times \mathcal{A} \rightarrow \mathbb{R}$, and a discount factor $\gamma \in [0, 1)$. Although we consider a known reward function, the main theoretical results can be easily extended to the case where it is learned alongside the transition function (see Appendix B.1). The one-step dynamics $p(s' | s, a)$ denote the probability of going from state s to state s' after taking action a . In general, the agent selects actions from a stochastic policy $\pi : \mathcal{S} \rightarrow \Delta(A)$ that defines the conditional probability distribution $\pi(a | s)$. At each time step, the agent is in some state s , selects an action $a \sim \pi(\cdot | s)$, receives a reward $r(s, a)$, and transitions to a next state $s' \sim p(\cdot | s, a)$. We define the value function

$V^{\pi,p} : \mathcal{S} \rightarrow \mathbb{R}$ of a policy π and transition function p as the expected sum of discounted rewards under the MDP dynamics,

$$V^{\pi,p}(s) = \mathbb{E}_{\tau \sim P} \left[\sum_{h=0}^{\infty} \gamma^h r(s_h, a_h) \mid s_0 = s \right], \quad (1)$$

where the expectation is taken under the random trajectories τ drawn from the trajectory distribution $P(\tau) = \prod_{h=0}^{\infty} \pi(a_h \mid s_h) p(s_{h+1} \mid s_h, a_h)$.

We consider a Bayesian setting similar to previous work by [17], [48], [11], in which the transition function p is a random variable with some known prior distribution $\Phi(p)$. As the agent interacts in \mathcal{M} , it collects data¹ \mathcal{D} and updates its posterior belief $\Phi(p \mid \mathcal{D})$ via Bayes' rule. In what follows, we omit further qualifications and refer to Φ as the posterior over transition functions. Such distribution over transition functions naturally induces a distribution over value functions. The main focus of this paper is to study methods that estimate the *variance* of the value function $V^{\pi,p}$ under Φ , namely $\mathbb{V}_{p \sim \Phi} [V^{\pi,p}(s)]$. Our theoretical results extend to state-action value functions (see Appendix B.2). The motivation behind studying this quantity is its potential for risk-aware optimization.

A method to estimate an upper-bound the variance of Q -values by solving a UBE was introduced by [11]. Their theory holds for a class of MDPs where the value functions and transition functions are uncorrelated. This family of MDPs is characterized by the following assumptions:

Assumption 1 (Parameter Independence [49]). *The posterior over the random vector $p(\cdot \mid s, a)$ is independent for each pair $(s, a) \in \mathcal{S} \times \mathcal{A}$.*

Assumption 2 (Acyclic MDP [17]). *For any realization of p , the MDP \mathcal{M} is a directed acyclic graph, i.e., states are not visited more than once in any given episode.*

Assumption 1 is satisfied when modelling state transitions as independent categorical random variables for every pair (s, a) , with the unknown parameter vector $p(\cdot \mid s, a)$ under a Dirichlet prior [49]. Assumption 2 is non-restrictive as any finite-horizon MDP with cycles can be transformed into an equivalent time-inhomogeneous MDP without cycles by adding a time-step variable h to the state-space. Since the state-space is finite-dimensional, for infinite-horizon problems we consider the existence of a terminal (absorbing) state that is reached within a finite number of steps. The direct consequence of these assumptions is that the random variables $V^{\pi,p}(s')$ and $p(s' \mid s, a)$ are independent (see Lemmas 2 and 3 in Appendix A.1 for a formal proof).

Other quantities of interest are the posterior mean transition function starting from the current state-action pair (s, a) ,

$$\bar{p}(\cdot \mid s, a) = \mathbb{E}_{p \sim \Phi} [p(\cdot \mid s, a)], \quad (2)$$

and the posterior mean value function for any $s \in \mathcal{S}$,

$$\bar{V}^{\pi}(s) = \mathbb{E}_{p \sim \Phi} [V^{\pi,p}(s)]. \quad (3)$$

Note that \bar{p} is a transition function that combines both aleatoric *and* epistemic uncertainty. Even if we limit the posterior Φ to only include deterministic transition functions,

1. We omit time-step subscripts and refer to dataset \mathcal{D} as the collection of all available transition data.

\bar{p} remains a stochastic transition function due to the epistemic uncertainty.

In [11], *local* uncertainty is defined as

$$w(s) = \mathbb{V}_{p \sim \Phi} \left[\sum_{a, s'} \pi(a \mid s) p(s' \mid s, a) \bar{V}^{\pi}(s') \right], \quad (4)$$

which captures variability of the posterior mean value function at the next state s' . Based on this local uncertainty, [11] proposes the UBE

$$W^{\pi}(s) = \gamma^2 w(s) + \gamma^2 \sum_{a, s'} \pi(a \mid s) \bar{p}(s' \mid s, a) W^{\pi}(s'), \quad (5)$$

that propagates the local uncertainty using the posterior mean dynamics. It was proven that the fixed-point solution of (5) is an upper-bound of the epistemic variance of the values, i.e., it satisfies $W^{\pi}(s) \geq \mathbb{V}_{p \sim \Phi} [V^{\pi,p}(s)]$ for all s .

3 UNCERTAINTY BELLMAN EQUATION

In this section, we build a new UBE whose fixed-point solution is *equal* to the variance of the value function and we show explicitly the gap between (5) and $\mathbb{V}_{p \sim \Phi} [V^{\pi,p}(s)]$.

The values $V^{\pi,p}$ are the fixed-point solution to the Bellman expectation equation, which relates the value of the current state s with the value of the next state s' . Further, under Assumptions 1 and 2, applying the expectation operator to the Bellman recursion results in $\bar{V}^{\pi}(s) = V^{\pi, \bar{p}}(s)$. The Bellman recursion propagates knowledge about the *local* rewards $r(s, a)$ over multiple steps, so that the value function encodes the *long-term* value of states if we follow policy π . Similarly, a UBE is a recursive formula that propagates a notion of *local uncertainty*, $u(s)$, over multiple steps. The fixed-point solution to the UBE, which we call the U -values, encodes the *long-term epistemic uncertainty* about the values of a given state.

Previous formulations by [17], [11] differ only on their definition of the local uncertainty and result on U -values that upper-bound the posterior variance of the values. The first key insight of our paper is that we can define u such that the U -values converge exactly to the variance of values. This result is summarized in the following theorem:

Theorem 1. *Under Assumptions 1 and 2, for any $s \in \mathcal{S}$ and policy π , the posterior variance of the value function, $U^{\pi} = \mathbb{V}_{p \sim \Phi} [V^{\pi,p}]$ obeys the uncertainty Bellman equation*

$$U^{\pi}(s) = \gamma^2 u(s) + \gamma^2 \sum_{a, s'} \pi(a \mid s) \bar{p}(s' \mid s, a) U^{\pi}(s'), \quad (6)$$

where $u(s)$ is the local uncertainty defined as

$$u(s) = \mathbb{V}_{a, s' \sim \pi, \bar{p}} [\bar{V}^{\pi}(s')] - \mathbb{E}_{p \sim \Phi} [\mathbb{V}_{a, s' \sim \pi, p} [V^{\pi,p}(s')]]. \quad (7)$$

Proof. See Appendix A.1. \square

One may interpret the U -values from Theorem 1 as the associated state-values of an alternate *uncertainty MDP*, $\mathcal{U} = \{\mathcal{S}, \mathcal{A}, \bar{p}, \rho, \gamma^2 u, \gamma^2\}$, where the agent receives uncertainty rewards and transitions according to the mean dynamics \bar{p} .

A key difference between u and w is how they represent epistemic uncertainty: in the former, it appears only within the first term, through the one-step variance over \bar{p} ; in the latter, the variance is computed over Φ . While the

two perspectives may seem fundamentally different, in the following theorem we present a clear relationship that connects Theorem 1 with the upper bound (5).

Theorem 2. *Under Assumptions 1 and 2, for any $s \in \mathcal{S}$ and policy π , it holds that $u(s) = w(s) - g(s)$, where $g(s) = \mathbb{E}_{p \sim \Phi} [\mathbb{V}_{a, s' \sim \pi, p} [V^{\pi, p}(s')] - \mathbb{V}_{a, s' \sim \pi, p} [\bar{V}^{\pi}(s')]]$. Furthermore, we have that the gap $g(s)$ is non-negative, thus $u(s) \leq w(s)$.*

Proof. See Appendix A.2. \square

The gap $g(s)$ of Theorem 2 can be interpreted as the *average difference* of aleatoric uncertainty about the next values with respect to the mean values. The gap vanishes only if the epistemic uncertainty goes to zero, or if the MDP and policy are both deterministic.

We directly connect Theorems 1 and 2 via the equality

$$\underbrace{\mathbb{V}_{a, s' \sim \pi, \bar{p}} [\bar{V}^{\pi}(s')]}_{\text{total}} = \underbrace{w(s)}_{\text{epistemic}} + \underbrace{\mathbb{E}_{p \sim \Phi} [\mathbb{V}_{a, s' \sim \pi, p} [\bar{V}^{\pi}(s')]]}_{\text{aleatoric}}, \quad (8)$$

which helps us analyze our theoretical results. The uncertainty reward defined in (7) has two components: the first term corresponds to the *total uncertainty* about the *mean* values of the next state, which is further decomposed in (8) into an epistemic and aleatoric components. When the epistemic uncertainty about the MDP vanishes, then $w(s) \rightarrow 0$ and only the aleatoric component remains. Similarly, when the MDP and policy are both deterministic, the aleatoric uncertainty vanishes and we have $\mathbb{V}_{a, s' \sim \pi, \bar{p}} [\bar{V}^{\pi}(s')] = w(s)$. The second term of (7) is the *average aleatoric uncertainty* about the value of the next state. When there is no epistemic uncertainty, this term is non-zero and exactly equal to the aleatoric term in (8) which means that $u(s) \rightarrow 0$. Thus, we can interpret $u(s)$ as a *relative local uncertainty* that subtracts the average aleatoric noise out of the total uncertainty around the mean values. Perhaps surprisingly, our theory allows negative $u(s)$ (see Section 3.1 for a concrete example).

Through Theorem 2 we provide an alternative proof of why the UBE (5) results in an upper-bound of the variance, specified by the next corollary.

Corollary 1. *Under Assumptions 1 and 2, for any $s \in \mathcal{S}$ and policy π , it holds that the solution to the uncertainty Bellman equation (5) satisfies $W^{\pi}(s) \geq U^{\pi}(s)$.*

Proof. The solution to the Bellman equations (5) and (6) are the value functions under some policy π of identical MDPs except for their reward functions. Given two identical MDPs \mathcal{M}_1 and \mathcal{M}_2 differing only on their corresponding reward functions r_1 and r_2 , if $r_1 \leq r_2$ for any input value, then for any trajectory τ we have that the returns (sum of discounted rewards) must obey $R_1(\tau) \leq R_2(\tau)$. Lastly, since the value functions V_1^{π}, V_2^{π} are defined as the expected returns under the same trajectory distribution, and the expectation operator preserves inequalities, then we have that $R_1(\tau) \leq R_2(\tau) \implies V_1^{\pi} \leq V_2^{\pi}$. \square

Corollary 1 reaches the same conclusions as [11], but it brings important explanations about their upper bound on the variance of the value function. First, by Theorem 2 the upper bound is a consequence of the over approximation

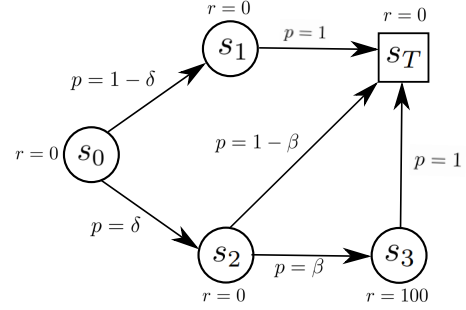


Fig. 1: Toy example Markov Reward Process. The random variables δ and β indicate epistemic uncertainty about the MRP. State s is an absorbing (terminal) state.

TABLE 1: Comparison of local uncertainty rewards and solutions to the UBE associated with the toy example from Figure 1. The U -values converge to the true posterior variance of the values, while W^{π} obtains an upper-bound.

States	$u(s)$	$w(s)$	$W^{\pi}(s)$	$U^{\pi}(s)$
s_0	-0.6	5.0	21.3	15.7
s_2	25.0	25.0	25.0	25.0

of the reward function used to solve the UBE. Second, the gap between the exact reward function $u(s)$ and the approximation $w(s)$ is fully characterized by $g(s)$ and brings interesting insights. In particular, the influence of the gap term depends on the stochasticity of the dynamics and the policy. In the limit, the term vanishes under deterministic transitions and action selection. In this scenario, the upper-bound found by [11] becomes tight.

Our method returns the exact *epistemic* uncertainty about the values by considering the inherent aleatoric uncertainty of the MDP and the policy. In a practical RL setting, disentangling the two sources of uncertainty is key for effective exploration. We are interested in exploring regions of high epistemic uncertainty, where new knowledge can be obtained. If the variance estimate fuses both sources of uncertainty, then we may be guided to regions of high uncertainty but with little information to be gained.

3.1 Toy Example

To illustrate the theoretical findings of this paper, consider the simple Markov reward process (MRP) of Figure 1. Assume δ and β to be random variables drawn from a discrete uniform distribution $\delta \sim \text{Unif}(\{0.7, 0.6\})$ and $\beta \sim \text{Unif}(\{0.5, 0.4\})$. As such, the distribution over possible MRPs is finite and composed of the four possible combinations of δ and β . Note that the example satisfies Assumptions 1 and 2. In Table 1 we include the results for the uncertainty rewards and solution to the respective UBEs (the results for s_1 and s_3 are trivially zero). For state s_2 , the upper-bound W^{π} is tight and we have $W^{\pi}(s_2) = U^{\pi}(s_2)$. In this case, the gap vanishes not because of lack of stochasticity, but rather due to lack of epistemic uncertainty about the next-state values. Indeed, the values for s_3 and s are independent of δ and β , which results in the gap terms for s_2 cancelling out. For state s_0 the gap is non-zero and W^{π} overestimates the variance of the value by $\sim 36\%$. Our UBE formulation prescribes a *negative* reward

Algorithm 1 Model-based Q -variance estimation

- 1: **Input:** Posterior MDP Γ , policy π .
 - 2: $\{p_i, r_i\}_{i=1}^N \leftarrow \text{sample_mdp}(\Gamma)$
 - 3: $Q^\pi, \{Q_i\}_{i=1}^N \leftarrow \text{solve_bellman}(\{p_i, r_i\}_{i=1}^N, \pi)$
 - 4: $\hat{U}^\pi \leftarrow \text{qvariance}(\{p_i, r_i, Q_i\}_{i=1}^N, \bar{Q}^\pi, \pi)$
-

to be propagated in order to obtain the correct posterior variance.

4 UNCERTAINTY-AWARE POLICY OPTIMIZATION

In this section, we propose techniques to leverage uncertainty quantification of Q -values for both online and offline RL problems. In what follows, we consider the general setting with unknown rewards and define Γ to be the posterior distribution over MDPs, from which we can sample both reward and transition functions. Define \hat{U}^π to be an estimate of the posterior variance over Q -values for some policy π . Then, we consider algorithms that perform policy updates via the following upper (or lower) confidence bound [31] type of optimization problem

$$\pi = \operatorname{argmax}_\pi \bar{Q}^\pi + \lambda \sqrt{\hat{U}^\pi}, \quad (9)$$

where \bar{Q}^π is the posterior mean value function and λ is a risk-awareness parameter. A positive λ corresponds to risk-seeking, optimistic exploration while negative λ denotes risk-averse, pessimistic anti-exploration.

Algorithm 1 describes our general framework to estimate \bar{Q}^π and \hat{U}^π : we sample an ensemble of N MDPs from the current posterior Γ in Line 2 and use it to solve the Bellman expectation equation in Line 3, resulting in an ensemble of N corresponding Q functions and the posterior mean \bar{Q}^π . Lastly, \hat{U}^π is estimated in Line 4 via a generic variance estimation method `qvariance`. In what follows, we provide concrete implementations of `qvariance` both in tabular and continuous problems.

4.1 Tabular Problems

For problems with tabular representations of the state-action space, we implement `qvariance` by directly solving the proposed UBE²(6), which we denote `exact-ube`. For this purpose, we impose a Dirichlet prior on the transition function and a standard Normal prior for the rewards [50], which leads to closed-form posterior updates. After sampling N times from the MDP posterior (Line 2), we obtain the Q -functions (Line 3) in closed-form by solving the corresponding Bellman equation. The uncertainty rewards are estimated via sample-based approximations of the expectations/variances therein. Lastly, we solve (9) via policy iteration until convergence is achieved or until a maximum number of steps is reached.

Practical bound. The choice of a Dirichlet prior violates Assumption 2. A challenge arises in this practical setting:

2. For the UBE-based methods we use the equivalent equations for Q -functions, see Appendix B.3 for details.

`exact-ube` may result in *negative* U -values, as a combination of (i) the assumptions not holding and (ii) the possibility of negative uncertainty rewards. While (i) cannot be easily resolved, we propose a practical upper-bound on the solution of (6) such that the resulting U -values are non-negative and hence interpretable as variance estimates. We consider the clipped uncertainty rewards $\tilde{u} = \max(u_{\min}, u(s))$ with corresponding U -values \tilde{U}^π . It is straightforward to prove that, if $u_{\min} = 0$, then $W^\pi(s) \geq \tilde{U}^\pi(s) \geq U^\pi(s)$, which means that using \tilde{U}^π still results in a tighter upper-bound on the variance than W^π , while preventing non-positive solutions to the UBE. In what follows, we drop this notation and assume all U -values are computed from clipped uncertainty rewards.

4.2 Continuous Problems

We tackle problems in continuous domains using neural networks for function approximation. The resulting architecture is named Q -Uncertainty Soft Actor-Critic (QU-SAC) which builds upon MBPO by [5] and is depicted in Figure 2.

Posterior dynamics. In contrast to the tabular implementation, maintaining an explicit distribution over MDPs from which we can sample is intractable. Instead, we approximate Γ with an ensemble, which have been linked to approximate posterior inference [51]. More concretely, we model Γ as a discrete uniform distribution of N probabilistic neural networks, denoted p_θ , that output the mean and covariance of a Gaussian distribution over next states and rewards [7]. In this case, the output of Line 2 in Algorithm 1 is precisely the ensemble of neural networks.

Critics. The original MBPO trains Q -functions represented as neural networks via TD-learning on data generated via *model-randomized* k -step rollouts from initial states that are sampled from \mathcal{D} . Each forward prediction of the rollout comes from a randomly selected model of the ensemble and the transitions are stored in a single replay buffer $\mathcal{D}_{\text{model}}$, which is then fed into a model-free optimizer like SAC. Algorithm 1 requires a few modifications from the MBPO methodology. To implement Line 3, in addition to $\mathcal{D}_{\text{model}}$, we create N new buffers $\{\mathcal{D}_i\}_{i=1}^N$ filled with *model-consistent* rollouts, where each k -step rollout is generated under a single model of the ensemble, starting from initial states sampled from \mathcal{D} . We train an ensemble of N value functions $\{Q_i\}_{i=1}^N$, parameterized by $\{\psi_i\}_{i=1}^N$, and minimize the residual Bellman error with entropy regularization

$$\mathcal{L}(\psi_i) = \mathbb{E}_{(s,a,r,s') \sim \mathcal{D}_i} \left[(y_i - Q_i(s, a; \psi_i))^2 \right], \quad (10)$$

where $y_i = r + \gamma \left(Q_i(s', a'; \bar{\psi}_i) - \alpha \log \pi_\phi(a' | s') \right)$ and $\bar{\psi}_i$ are the target network parameters updated via Polyak averaging for stability during training [43]. The mean Q -values, \bar{Q}^π , are estimated as the average value of the Q -ensemble.

Uncertainty rewards. Our theory prescribes propagating the uncertainty rewards (7) to obtain the `exact-ube` estimate. It is possible to approximate these rewards, as in the tabular case, by considering the ensemble of critics as samples

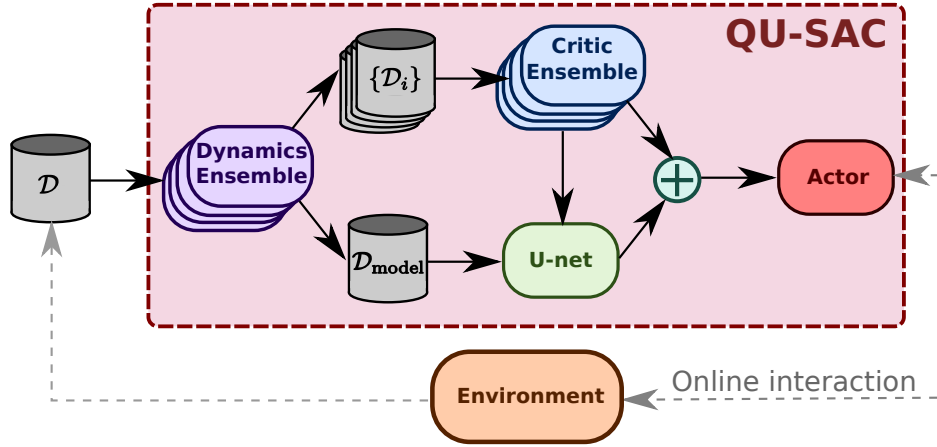


Fig. 2: Architecture for Q -Uncertainty Soft Actor-Critic (QU-SAC). The dataset \mathcal{D} may be either static, as in offline RL, or be dynamically populated with online interactions. This dataset is used to train an ensemble of dynamics models which is then used for synthetic rollout generation. Each member of the ensemble populates its own buffer \mathcal{D}_i , which is used to train a corresponding ensemble of critics. Additionally, member-randomized rollouts are stored in $\mathcal{D}_{\text{model}}$ and used to train a U -net, which outputs an estimated epistemic variance of the value prediction. Lastly, the actor aims to optimize the risk-aware objective (9), which combines the output of the critic ensemble and the U -net.

from the value distribution. If we focus only on estimating the positive component of the `exact-ube` estimate, i.e., the local uncertainty defined by [11], then a sample-based approximation is given by

$$\hat{w}(s, a) = \mathbb{V}_i \left[\left\{ \bar{Q}(s'_i, a'_i) \right\}_{i=1}^N \right], \quad (11)$$

where $s'_i \sim p_i(\cdot | s, a)$. While this approach is sensible from our theory perspective and has led to promising results in our previous work [20], it has two main shortcomings in practice: (i) it can be computationally intensive to estimate the rewards and (ii) the magnitude of the rewards is typically low, even if the individual critics have largely different estimated values. The latter point is illustrated in Figure 3: the term $\hat{w}(s, a)$ captures the local variance of the average value function, which would be small if the function is relatively flat around (s, a) or if the dynamics model ensemble yields similar forward predictions starting from (s, a) . Empirically, we found that across many environments the average magnitude of $\hat{w}(s, a)$ is indeed small (e.g., $\sim 10^{-3}$), which makes training a U -net challenging mainly due to vanishing gradients from the *softplus* layer. We alleviate both shortcomings via a simple proxy uncertainty reward:

$$\hat{w}_{\text{ub}}(s, a) = \mathbb{V}_i \left[\left\{ Q_i(s, a) \right\}_{i=1}^N \right], \quad (12)$$

which is the sample-based approximation of the value variance. We denote this estimate `upper-bound` (thus, the subscript “ub” in (12)), since in the limit of infinite samples from the value distribution, solving a UBE with rewards $\hat{w}_{\text{ub}}(s, a)$ results in an upper bound on the value variance at (s, a) .

The proxy rewards $\hat{w}_{\text{ub}}(s, a)$ capture explicitly the value ensemble disagreement rather than local variations of the average value, which empirically results in larger rewards being propagated through the UBE. Moreover, the proxy reward calculation requires only one forward pass through the critic ensemble, without need for forward predictions with the dynamics model as for $\hat{w}(s, a)$.

Variance estimate. Similar to critic training, we model the variance estimate \hat{U}^π with a neural network, denoted U -net, parameterized by φ and trained to minimize the UBE residual

$$\mathcal{L}(\varphi) = \mathbb{E}_{(s, a, r, s') \sim \mathcal{D}_{\text{model}}} \left[(z - U(s, a; \varphi))^2 \right], \quad (13)$$

with targets $z = \gamma^2 \hat{w}_{\text{ub}}(s, a) + \gamma^2 U(s', a'; \bar{\varphi})$ and target parameters $\bar{\varphi}$ updated like in regular critics. Since we interpret the output of the network as predictive variances, we use a *softplus* output layer to guarantee non-negative values. Moreover, we apply a symlog transformation to the UBE targets z , as proposed by [52], which helps the U -net converge to the target values more easily. Namely, the U -net is trained to predict the symlog transform of the target values z , defined as $\text{symlog}(z) = \text{sign}(z) \log(|z| + 1)$. To retrieve the U -values, we apply the inverse transform $\text{symexp}(z) = \text{sign}(z)(\exp(|z|) - 1)$ to the output of the U -net.

Actor. The stochastic policy is represented as a neural network with parameters ϕ , denoted by π_ϕ . The policy’s objective is derived from SAC, where in addition to entropy regularization, we include the predicted standard deviation of values for uncertainty-aware optimization.

$$\mathcal{L}(\phi) = \mathbb{E}_{s \sim \mathcal{D}_{\text{model}}} \left\{ \mathbb{E}_{a \sim \pi_\phi} \left\{ \bar{Q}(s, a) + \lambda \sqrt{U(s, a)} - \alpha \log \pi_\phi(a | s) \right\} \right\}. \quad (14)$$

Online vs offline optimization. With QU-SAC we aim to use largely the same algorithm to tackle both online and offline problems. Beyond differences in hyperparameters, the only algorithmic change in QU-SAC is that for offline optimization we modify the data used to train the actor, critic and U -net to also include data from the offline dataset (an even 50/50

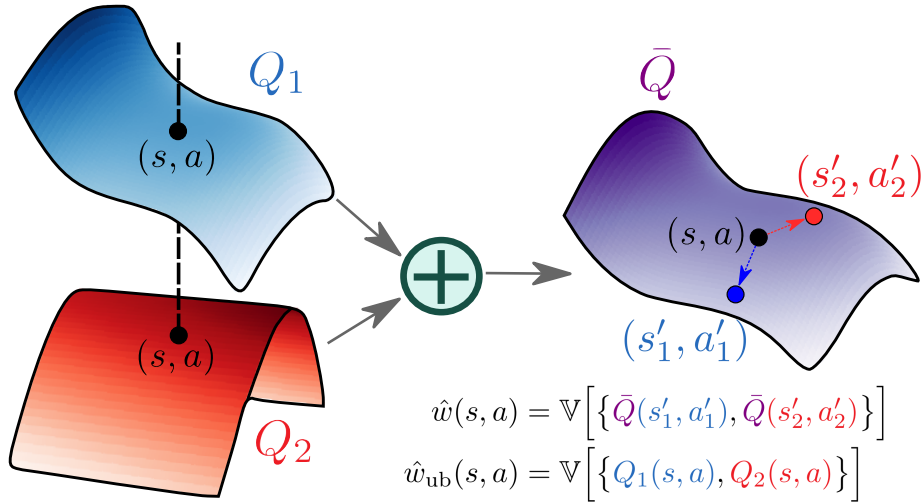


Fig. 3: Illustrative example of uncertainty rewards. **(Left)** ensemble of two value functions $\{Q_1, Q_2\}$. **(Right)** corresponding mean value function \bar{Q} . The theory prescribes estimating the term in (4), denoted $\hat{w}(s, a)$, which captures local variability of \bar{Q} around (s, a) . Empirically, $\hat{w}(s, a)$ can be small despite large differences in individual members of the value ensemble, e.g., because \bar{Q} is relatively flat around (s, a) . We propose the proxy uncertainty reward $\hat{w}_{\text{ub}}(s, a)$ which directly captures variability across the value ensemble and is less computationally expensive (no dynamics model forward pass).

split between offline and model-generated data in our case), which is a standard practice in offline model-based RL [39], [12], [38], [40].

5 EXPERIMENTS

In this section, we empirically evaluate the performance of our risk-aware policy optimization scheme (9) in various problems and compare against related baselines.

5.1 Baselines

In Algorithm 1, we consider different implementations of the variance method to estimate $\hat{U}(s, a)$: `ensemble-var` directly uses the sample-based approximation $\hat{w}_{\text{ub}}(s, a)$ in (12); `pombu` uses the solution to the UBE (5); `exact-ube` uses the solution to our proposed UBE (6); and `upper-bound` refers to the solution of the UBE with the modified rewards (12). We also compare against not using any form of uncertainty quantification, which we refer to as `ensemble-mean`.

Additionally, in tabular problems we include PSRL by [53] as a baseline since it typically outperforms recent OFU-based methods [48], [54]. We also include MBPO [5] and MOPO [12] as baselines for online and offline problems, respectively.

5.2 Gridworld Exploration Benchmark

We evaluate the tabular implementation in grid-world environments where exploration is key to find the optimal policy.

DeepSea. First proposed by [55], this environment tests the agent’s ability to explore over multiple time steps in the presence of a deterrent. It consists of an $L \times L$ grid-world MDP, where the agent starts at the top-left cell and must reach the lower-right cell. The agent decides to move left or right, while always descending to the row below. We consider

the deterministic version of the problem, so the agent always transitions according to the chosen action. Going left yields no reward, while going right incurs an action cost (negative reward) of $0.01/L$. The bottom-right cell yields a reward of 1, so that the optimal policy is to always go right. As the size of the environment increases, the agent must perform sustained exploration in order to reach the sparse reward. Detailed implementation and hyperparameter details are included in Appendix C.1.

The experiment consists on running each method for 1000 episodes and five random seeds, recording the total regret and “learning time”, defined as the first episode where the rewarding state has been found at least in 10% of the episodes so far [48]. For this experiment, we found that using $u_{\text{min}} = -0.05$ improves the performance of our method: since the underlying MDP is acyclic, propagating negative uncertainty rewards is consistent with our theory.

Figure 4 (left) shows the evolution of learning time as L increases. Our method achieves the lowest learning time and best scaling with problem size. Notably, all the OFU-based methods learn faster than PSRL, a strong argument in favour of using the variance of value functions to guide exploration. Figure 4 (right) shows that our approach consistently achieves the lowest total regret across all values of L . This empirical evidence indicates that the solution to our UBE can be integrated into common exploration techniques like UCB to serve as an effective uncertainty signal. Moreover, our method significantly improves performance over `pombu`, highlighting the relevance of our theory results.

Detailed results of all the runs are included in Section C.3.1. Additional ablation studies on different estimates for our UBE and exploration gain λ are included in Sections C.3.2 and C.3.4, respectively.

7-room. As implemented by [56], the 7-room environment consists of seven connected rooms of size 5×5 . The agent

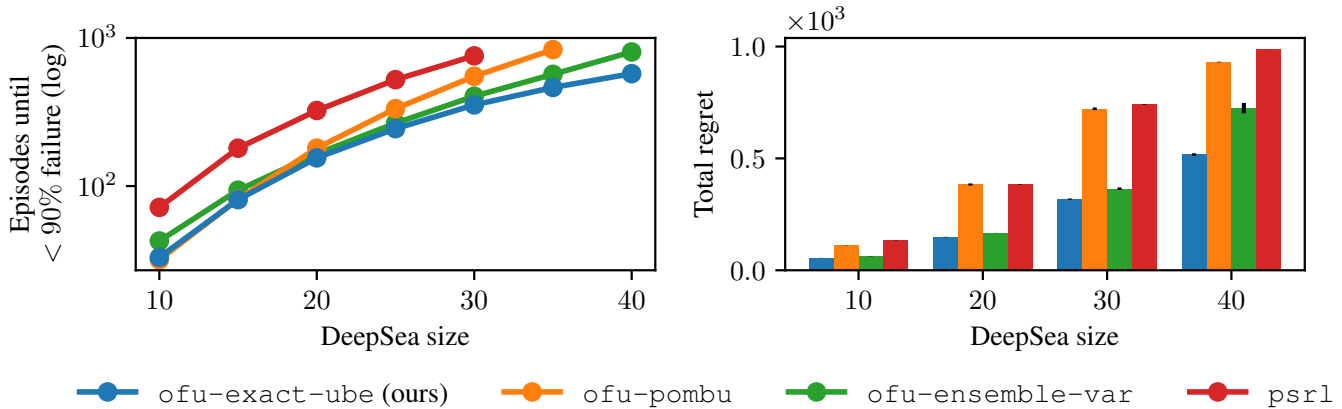


Fig. 4: Performance in the *DeepSea* benchmark. Lower values in plots indicate better performance. (Left) Learning time is measured as the first episode where the sparse reward has been found at least in 10% of episodes so far. (Right) Total regret is approximately equal to the number of episodes where the sparse reward was not found. Results represent the average over 5 random seeds, and vertical bars on total regret indicate the standard error. Our variance estimate achieves the lowest regret and best scaling with problem size.

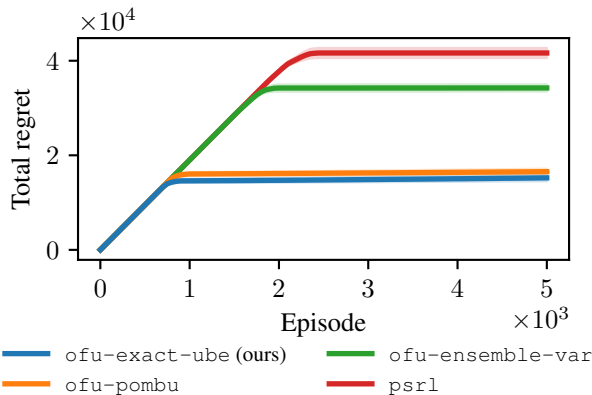


Fig. 5: Total regret curve for the 7-room environment. Lower regret is better. Results are the average (solid lines) and standard error (shaded regions) over 10 random seeds. Our method achieves the lowest regret, significantly outperforming PSRL.

starts in the center of the middle room and an episode lasts 40 steps. The possible actions are up-down-left-right and the agent transitions according to the selected action with probability 0.95, otherwise it lands in a random neighboring cell. The environment has zero reward everywhere except two small rewards at the start position and in the left-most room, and one large reward in the right-most room. Unlike *DeepSea*, the underlying MDP for this environment contains cycles, so it evaluates our method beyond the theoretical assumptions. In Figure 5, we show the regret curves over 5000 episodes. Our method achieves the lowest regret, which is remarkable considering recent empirical evidence favoring PSRL over OFU-based methods in these type of environments [54]. The large gap between *ensemble-var* and the UBE-based methods is due to overall larger variance estimates from the former, which consequently requires more episodes to reduce the value uncertainty.

5.3 DeepMind Control Suite - Exploration Benchmark

In this section, we evaluate the performance of QU-SAC for online exploration in environments with continuous state-action spaces. Implementation details and hyperparameters are included in Appendix D.

We test the exploration capabilities of QU-SAC on a subset of environments from the DeepMind Control (DMC) suite [18] with a sparse reward signal. Moreover, we modify the environments' rewards to include a small negative term proportional to the squared norm of the action vector, similar to [8]. Such action costs are relevant for energy-constrained systems where the agent must learn to maximize the primary objective while minimizing the actuation effort. However, the added negative reward signal may inhibit exploration and lead to premature convergence to sub-optimal policies. In this context, we want to compare the exploration capabilities of QU-SAC with the different variance estimates.

In Figure 6 we plot the performance of all baselines in our exploration benchmark after 500 episodes (or equivalently, 500K environment steps). In addition to individual learning curves, we aggregate performance across all environments and report the median and inter-quartile mean (IQM) [57]. The results highlight that QU-SAC with our proposed upper-bound variance estimate offers the best overall performance. The pendulum swingup environment is a prime example of a task where the proposed approach excels: greedily optimizing for mean values, like MBPO and *ensemble-mean*, does not explore enough to observe the sparse reward; *ensemble-var* improves performance upon the greedy approach, but does not work consistently across random seeds unlike *upper-bound*. In this case, the stronger exploration signal afforded by propagating uncertainty through the *U-net* is key to maintain exploration despite low variability on the critic ensemble predictions.

5.4 D4RL Offline Benchmark

In this section, we evaluate the performance of QU-SAC for offline RL in the Mujoco [58] datasets from the D4RL bench-

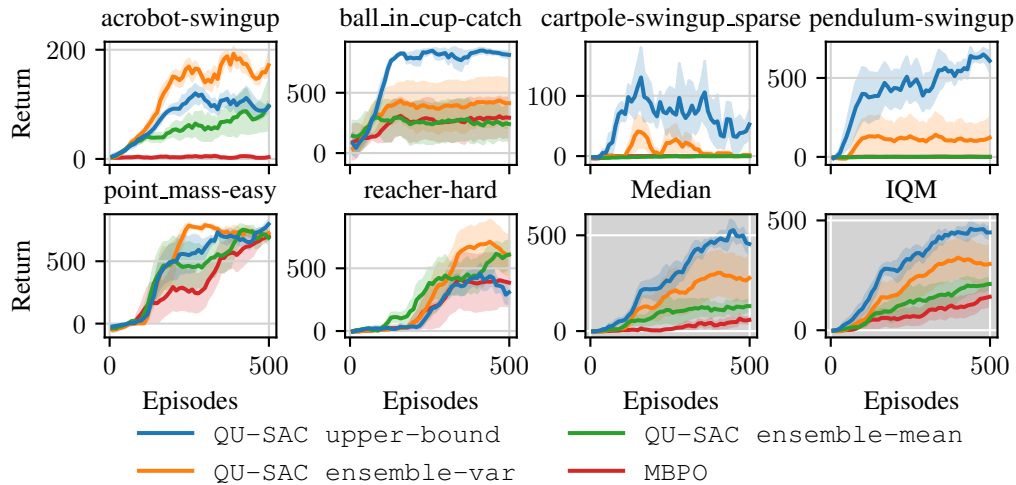


Fig. 6: DeepMind Control Suite Benchmark smoothed learning curves over 500 episodes (500K environment steps). We report the mean (solid) and standard error (shaded region) over five random seeds. QU-SAC with the `upper-bound` variance estimate outperforms the baselines in 4/6 environments and has the best overall performance.

mark [19]. Implementation details and hyperparameters are included in Appendix E.

The core idea behind QU-SAC for offline optimization is to leverage the predicted value uncertainty for conservative (pessimistic) policy optimization. This simply involves fixing $\lambda < 0$ to downweight values depending on their predicted uncertainty. In addition to uncertainty-based pessimism, prior work proposed SAC- M [59] which uses an ensemble of M critics and imposes conservatism by taking the minimum of the ensemble prediction as the value estimate. A key question we want to address with our experiments is whether pure uncertainty-based pessimism is enough to avoid out-of-distribution over-estimation in offline RL.

In order to provide an empirical answer, we augment QU-SAC with SAC- M by training M critics for each of the N dynamics models. The result is an ensemble of NM critics, labelled as Q_{ij} for $i = \{1, \dots, N\}$, $j = \{1, \dots, M\}$. Each subset of M critics is trained using clipped Q-learning [60] as in SAC- M , where the i -th critic prediction is simply defined as $Q_i(s, a) = \min_j Q_{ij}(s, a)$. The mean critic prediction is redefined as the average over clipped Q -values, $\bar{Q}(s, a) = 1/N \sum_{i=1}^N \min_j Q_{ij}(s, a)$. If $M = 1$ we recover the original QU-SAC which only uses variance prediction as a mechanism for conservative optimization. Note that MOPO fixes $M = 2$, which means it combines uncertainty and clipped-based conservatism by default; we re-implemented MOPO in order to allow for arbitrary M . In this context, our key question becomes: can any of the methods perform well with $M = 1$, i.e., only using uncertainty-based pessimism?

We conduct experiments in D4RL for three environments (Hopper, HalfCheetah and Walker2D) and four tasks each (random, medium, medium-replay and medium-expert) for a total of 12 datasets. For each dataset, we pre-train an ensemble of dynamics models and then run offline optimization for 1M gradient steps. In Figure 7 we present the results for the Hopper datasets using $M = \{1, 2\}$. In the pure uncertainty-based pessimism setting ($M = 1$), QU-SAC with the `upper-bound` variance estimate obtains the best performance by a wide margin. Qualitatively, the

effect of supplementing `upper-bound` with clipped Q-learning ($M = 2$) is more stable performance rather than a significant score improvement, unlike most other baselines that do improve substantially. These results suggest that proper uncertainty quantification might be sufficient for offline learning, without relying on additional mechanisms to combat out-of-distribution biases such as clipped Q-learning. Learning curves and scores for all datasets are provided in Appendix E.

In Table 2, we compare the final scores of QU-SAC (using `upper-bound` and $M = 2$) against recent model-based offline RL methods. While scores are typically lower than the state-of-the-art method CBOP [40], our general-purpose method outperforms MOPO and is on-par with more recent and stronger model-based baselines like COMBO and RAMBO³.

6 CONCLUSIONS

In this paper, we derived an uncertainty Bellman equation whose fixed-point solution converges to the variance of values given a posterior distribution over MDPs. Our theory brings new understanding by characterizing the gap in previous UBE formulations that upper-bound the variance of values. We showed that this gap is the consequence of an over-approximation of the uncertainty rewards being propagated through the Bellman recursion, which ignore the inherent *aleatoric* uncertainty from acting in an MDP. Instead, our theory recovers exclusively the *epistemic* uncertainty due to limited environment data, thus serving as an effective exploration signal. The tighter variance estimate showed improved regret in typical tabular exploration problems.

Beyond tabular RL, we identified challenges on applying the UBE theory for uncertainty quantification and proposed a simple proxy uncertainty reward to overcome them. Based

3. When $M = 1$, QU-SAC using `upper-bound` obtains an average score of 70.4 (IQM of 74.4) (see Table 5 in the supplementary material), which is also comparable to the reported performance of COMBO and RAMBO.

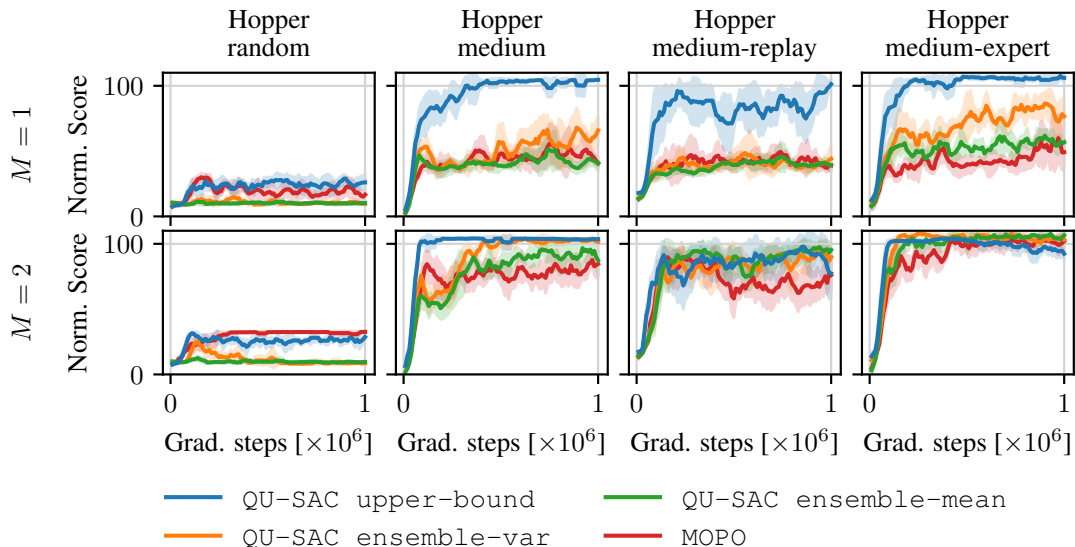


Fig. 7: D4RL learning curves for Hopper datasets, smoothed by a moving average filter. We report the mean (solid) and standard deviation (shaded region) over five random seeds of the average normalized score over 10 evaluation episodes. We use $M = 1$ for all baselines on the top row plots and $M = 2$ on the bottom row. QU-SAC with the `upper-bound` variance estimate provides the most consistent performance across both values of M .

TABLE 2: D4RL final normalized scores for model-based RL algorithms. The highest average scores are highlighted in light blue. MOPO* corresponds to our own implementation of the algorithm by [12], while QU-SAC utilizes the `upper-bound` variance estimate and $M = 2$. For MOPO* and QU-SAC, we report the mean and standard deviation over five random seeds. The scores for the original MOPO results are as reported by [37]. We take the results for COMBO [38], RAMBO [39] and CBOP [40] from their corresponding papers.

		MOPO	MOPO*	COMBO	RAMBO	CBOP	QU-SAC
Random	HalfCheetah	35.9±2.9	25.9±1.4	38.8±3.7	40.0 ±2.3	32.8±0.4	30.2±1.5
	Hopper	16.7±12.2	32.6 ±0.2	17.9±1.4	21.6±8.0	31.4±0.0	31.5±0.2
	Walker2D	4.2±5.7	1.0±1.9	7.0±3.6	11.5±10.5	17.8±0.4	21.7 ±0.1
Medium	HalfCheetah	73.1±2.4	60.6±2.4	54.2±1.5	77.6 ±1.5	74.3±0.2	60.7±1.7
	Hopper	38.3±34.9	81.3±15.7	97.2±2.2	92.8±6.0	102.6±0.1	103.5 ±0.2
	Walker2D	41.2±30.8	85.3±1.3	81.9±2.8	85.0±15.0	95.5 ±0.4	86.5±0.7
Medium Replay	HalfCheetah	69.2 ±1.1	55.7±0.9	55.1±1.0	68.9±2.3	66.4±0.3	58.9±1.3
	Hopper	32.7±9.4	69.0±27.0	89.5±2.8	96.6±7.0	104.3 ±0.4	86.2±20.9
	Walker2D	73.7±9.4	83.1±5.0	56.0±8.6	85.0±15.0	92.7 ±0.9	76.8±0.6
Medium Expert	HalfCheetah	70.3±21.9	95.0±1.7	90.0±5.6	93.7±10.5	105.4 ±1.6	99.1±2.5
	Hopper	60.6±32.5	104.5±7.7	111.1 ±2.9	83.3±9.1	111.6 ±0.2	93.8±10.4
	Walker2D	77.4±27.9	107.7±0.8	103.3±5.6	68.3±20.6	117.2 ±0.5	93.7±25.6
Average		49.4	66.8	66.8	68.7	79.3	70.2
IQM		52.6	72.5	71.1	78.0	89.3	77.1

on this approximation, we introduced the Q -Uncertainty Soft Actor-Critic (QU-SAC) algorithm that can be used for both online and offline RL with minimal changes. For online RL, the proposed proxy uncertainty reward was instrumental for exploration in sparse reward problems. In offline RL, we demonstrate QU-SAC has solid performance without additional regularization mechanisms unlike other uncertainty quantification methods.

REFERENCES

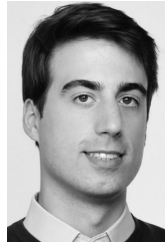
- [1] R. Sutton and A. Barto, *Reinforcement Learning: An Introduction*. MIT Press, 2018, vol. 7, issue: 2 Pages: 548.
- [2] R. S. Sutton, “Dyna, an Integrated Architecture for Learning, Planning, and Reacting,” *ACM SIGART Bulletin*, vol. 2, no. 4, pp. 160–163, Jul. 1991.
- [3] A. L. Strehl and M. L. Littman, “An Analysis of Model-Based Interval Estimation for Markov Decision Processes,” *Journal of Computer and System Sciences*, vol. 74, no. 8, pp. 1309–1331, 2008, publisher: Elsevier.
- [4] T. Jaksch, R. Ortner, and P. Auer, “Near-optimal Regret Bounds for Reinforcement Learning,” *Journal of Machine Learning Research*, vol. 11, no. 4, 2010.
- [5] M. Janner, J. Fu, M. Zhang, and S. Levine, “When to Trust Your Model: Model-Based Policy Optimization,” in *Advances in Neural Information Processing Systems*, vol. 32. Curran Associates, Inc., 2019.
- [6] S. Depeweg, J.-M. Hernandez-Lobato, F. Doshi-Velez, and S. Udluft,

- “Decomposition of Uncertainty in Bayesian Deep Learning for Efficient and Risk-sensitive Learning,” in *International Conference on Machine Learning*. PMLR, Jul. 2018, pp. 1184–1193, iSSN: 2640-3498.
- [7] K. Chua, R. Calandra, R. McAllister, and S. Levine, “Deep Reinforcement Learning in a Handful of Trials using Probabilistic Dynamics Models,” in *Advances in Neural Information Processing Systems*, vol. 31, 2018, arXiv: 1805.12114.
- [8] S. Curi, F. Berkenkamp, and A. Krause, “Efficient Model-Based Reinforcement Learning through Optimistic Policy Search and Planning,” in *Advances in Neural Information Processing Systems*, vol. 33. Curran Associates, Inc., 2020, pp. 14 156–14 170.
- [9] M. P. Deisenroth and C. E. Rasmussen, “PILCO: A Model-Based and Data-Efficient Approach to Policy Search,” in *International Conference on Machine Learning*, 2011, pp. 465–472.
- [10] Y. Fan and Y. Ming, “Model-based Reinforcement Learning for Continuous Control with Posterior Sampling,” in *International Conference on Machine Learning*, ser. Proceedings of Machine Learning Research, vol. 139. PMLR, Jul. 2021, pp. 3078–3087.
- [11] Q. Zhou, H. Li, and J. Wang, “Deep Model-Based Reinforcement Learning via Estimated Uncertainty and Conservative Policy Optimization,” in *AAAI Conference on Artificial Intelligence*, vol. 34, Apr. 2020, pp. 6941–6948.
- [12] T. Yu, G. Thomas, L. Yu, S. Ermon, J. Y. Zou, S. Levine, C. Finn, and T. Ma, “MOPO: Model-based Offline Policy Optimization,” in *Advances in Neural Information Processing Systems*, vol. 33. Curran Associates, Inc., 2020, pp. 14 129–14 142.
- [13] M. G. Bellemare, W. Dabney, and R. Munos, “A Distributional Perspective on Reinforcement Learning,” in *International Conference on Machine Learning*, ser. Proceedings of Machine Learning Research, D. Precup and Y. W. Teh, Eds., vol. 70. PMLR, Aug. 2017, pp. 449–458.
- [14] H. Eriksson, D. Basu, M. Alibeigi, and C. Dimitrakakis, “SENTINEL: taming uncertainty with ensemble based distributional reinforcement learning,” in *Conference on Uncertainty in Artificial Intelligence*, ser. Proceedings of Machine Learning Research, J. Cussens and K. Zhang, Eds., vol. 180. PMLR, Aug. 2022, pp. 631–640.
- [15] T. Moskovitz, J. Parker-Holder, A. Pacchiano, M. Arbel, and M. Jordan, “Tactical Optimism and Pessimism for Deep Reinforcement Learning,” in *Advances in Neural Information Processing Systems*, vol. 34. Curran Associates, Inc., 2021, pp. 12 849–12 863.
- [16] D. Schneegass, A. Hans, and S. Udluft, “Uncertainty in Reinforcement Learning-Awareness, Quantisation, and Control,” *Robot Learning, Sciyo*, pp. 65–90, 2010.
- [17] B. O’Donoghue, I. Osband, R. Munos, and V. Mnih, “The Uncertainty Bellman Equation and Exploration,” in *International Conference on Machine Learning*, 2018, pp. 3836–3845.
- [18] S. Tunyasuvunakool, A. Muldal, Y. Doron, S. Liu, S. Bohez, J. Merel, T. Erez, T. Lillicrap, N. Heess, and Y. Tassa, “dm_control: Software and tasks for continuous control,” *Software Impacts*, vol. 6, p. 100022, 2020.
- [19] J. Fu, A. Kumar, O. Nachum, G. Tucker, and S. Levine, “D4RL: Datasets for Deep Data-Driven Reinforcement Learning,” 2020, eprint: 2004.07219.
- [20] C. E. Luis, A. G. Bottero, J. Vinogradska, F. Berkenkamp, and J. Peters, “Model-Based Uncertainty in Value Functions,” in *International Conference on Artificial Intelligence and Statistics*, ser. Proceedings of Machine Learning Research, F. Ruiz, J. Dy, and J.-W. van de Meent, Eds., vol. 206. PMLR, Apr. 2023, pp. 8029–8052.
- [21] R. Dearden, N. Friedman, and S. Russell, “Bayesian Q-Learning,” in *AAAI Conference on Artificial Intelligence*, ser. AAAI ’98/IAAI ’98. USA: American Association for Artificial Intelligence, 1998, pp. 761–768, event-place: Madison, Wisconsin, USA.
- [22] Y. Engel, S. Mannor, and R. Meir, “Bayes Meets Bellman: The Gaussian Process Approach to Temporal Difference Learning,” in *International Conference on Machine Learning*. AAAI Press, 2003, pp. 154–161.
- [23] I. Osband, C. Blundell, A. Pritzel, and B. Van Roy, “Deep Exploration via Bootstrapped DQN,” in *Advances in Neural Information Processing Systems*, vol. 29. Curran Associates, Inc., 2016.
- [24] E. Jorge, H. Eriksson, C. Dimitrakakis, D. Basu, and D. Grover, “Inferential Induction: A Novel Framework for Bayesian Reinforcement Learning,” in *Proceedings on “I Can’t Believe It’s Not Better!” at NeurIPS Workshops*, ser. Proceedings of Machine Learning Research, vol. 137. PMLR, Dec. 2020, pp. 43–52.
- [25] A. M. Metelli, A. Likmeta, and M. Restelli, “Propagating Uncertainty in Reinforcement Learning via Wasserstein Barycenters,” in *Advances in Neural Information Processing Systems*, vol. 32. Curran Associates, Inc., 2019.
- [26] M. Fellows, K. Hartikainen, and S. Whiteson, “Bayesian Bellman Operators,” in *Advances in Neural Information Processing Systems*, vol. 34. Curran Associates, Inc., 2021, pp. 13 641–13 656.
- [27] B. Lakshminarayanan, A. Pritzel, and C. Blundell, “Simple and Scalable Predictive Uncertainty Estimation using Deep Ensembles,” in *Advances in Neural Information Processing Systems*, vol. 30. Curran Associates, Inc., 2017.
- [28] J. Buckman, D. Hafner, G. Tucker, E. Brevdo, and H. Lee, “Sample-Efficient Reinforcement Learning with Stochastic Ensemble Value Expansion,” in *Advances in Neural Information Processing Systems*, vol. 31. Curran Associates, Inc., 2018.
- [29] B. Zhou, H. Zeng, F. Wang, Y. Li, and H. Tian, “Efficient and Robust Reinforcement Learning with Uncertainty-based Value Expansion,” *arXiv:1912.05328 [cs]*, Dec. 2019, arXiv: 1912.05328.
- [30] R. Kidambi, A. Rajeswaran, P. Netrapalli, and T. Joachims, “MOREL: Model-Based Offline Reinforcement Learning,” in *Advances in Neural Information Processing Systems*, vol. 33. Curran Associates, Inc., 2020, pp. 21 810–21 823.
- [31] P. Auer and R. Ortner, “Logarithmic Online Regret Bounds for Undiscounted Reinforcement Learning,” in *Advances in Neural Information Processing Systems*, vol. 19. MIT Press, 2006.
- [32] I. Osband and B. Van Roy, “Why is Posterior Sampling Better than Optimism for Reinforcement Learning?” in *International Conference on Machine Learning*. PMLR, 2017, pp. 2701–2710.
- [33] K. Ciosek, Q. Vuong, R. Loftin, and K. Hofmann, “Better Exploration with Optimistic Actor Critic,” in *Advances in Neural Information Processing Systems*, vol. 32. Curran Associates, Inc., 2019.
- [34] R. Y. Chen, S. Sidor, P. Abbeel, and J. Schulman, “UCB Exploration via Q-Ensembles,” *arXiv:1706.01502 [cs, stat]*, Nov. 2017, arXiv: 1706.01502.
- [35] S. Levine, A. Kumar, G. Tucker, and J. Fu, “Offline Reinforcement Learning: Tutorial, Review, and Perspectives on Open Problems,” *arXiv:2005.01643 [cs, stat]*, Nov. 2020, arXiv: 2005.01643.
- [36] A. Kumar, A. Zhou, G. Tucker, and S. Levine, “Conservative Q-Learning for Offline Reinforcement Learning,” in *Advances in Neural Information Processing Systems*, H. Larochelle, M. Ranzato, R. Hadsell, M. F. Balcan, and H. Lin, Eds., vol. 33. Curran Associates, Inc., 2020, pp. 1179–1191.
- [37] C. Bai, L. Wang, Z. Yang, Z.-H. Deng, A. Garg, P. Liu, and Z. Wang, “Pessimistic Bootstrapping for Uncertainty-Driven Offline Reinforcement Learning,” in *International Conference on Learning Representations*, Mar. 2022.
- [38] T. Yu, A. Kumar, R. Rafailov, A. Rajeswaran, S. Levine, and C. Finn, “COMBO: Conservative Offline Model-Based Policy Optimization,” in *Advances in Neural Information Processing Systems*, M. Ranzato, A. Beygelzimer, Y. Dauphin, P. S. Liang, and J. W. Vaughan, Eds., vol. 34. Curran Associates, Inc., 2021, pp. 28 954–28 967.
- [39] M. Rigter, B. Lacerda, and N. Hawes, “RAMBO-RL: Robust Adversarial Model-Based Offline Reinforcement Learning,” in *Advances in Neural Information Processing Systems*, Oct. 2022.
- [40] J. Jeong, X. Wang, M. Gimelfarb, H. Kim, B. Abdulhai, and S. Sanner, “Conservative Bayesian Model-Based Value Expansion for Offline Policy Optimization,” in *International Conference on Learning Representations*, Feb. 2023.
- [41] M. J. Sobel, “The Variance of Discounted Markov Decision Processes,” *Journal of Applied Probability*, vol. 19, no. 4, pp. 794–802, 1982, publisher: Cambridge University Press.
- [42] A. Tamar, D. Di Castro, and S. Mannor, “Temporal Difference Methods for the Variance of the Reward To Go,” in *International Conference on Machine Learning*. PMLR, 2013, pp. 495–503.
- [43] V. Mnih, K. Kavukcuoglu, D. Silver, A. Graves, I. Antonoglou, D. Wierstra, and M. Riedmiller, “Playing Atari with Deep Reinforcement Learning,” in *NIPS Deep Learning Workshop*, Dec. 2013, arXiv: 1312.5602.
- [44] E. Markou and C. E. Rasmussen, “Bayesian Methods for Efficient Reinforcement Learning in Tabular Problems,” in *NeurIPS Workshop on Biological and Artificial RL*, 2019.
- [45] J. Schulman, F. Wolski, P. Dhariwal, A. Radford, and O. Klimov, “Proximal Policy Optimization Algorithms,” *arXiv:1707.06347 [cs]*, Aug. 2017, arXiv: 1707.06347.

- [46] T. Haarnoja, A. Zhou, P. Abbeel, and S. Levine, "Soft Actor-Critic: Off-Policy Maximum Entropy Deep Reinforcement Learning with a Stochastic Actor," in *International Conference on Machine Learning*, vol. 80. PMLR, Jul. 2018, pp. 1861–1870.
- [47] L. Froehlich, M. Lefarov, M. Zeilinger, and F. Berkenkamp, "On-Policy Model Errors in Reinforcement Learning," in *International Conference on Learning Representations*, 2022.
- [48] B. O'Donoghue, "Variational Bayesian Reinforcement Learning with Regret Bounds," in *Advances in Neural Information Processing Systems*, vol. 34. Curran Associates, Inc., 2021, pp. 28 208–28 221.
- [49] R. Dearden, N. Friedman, and D. Andre, "Model Based Bayesian Exploration," in *Conference on Uncertainty in Artificial Intelligence*, ser. UAI'99. San Francisco, CA, USA: Morgan Kaufmann Publishers Inc., 1999, pp. 150–159, event-place: Stockholm, Sweden.
- [50] B. O'Donoghue, I. Osband, and C. Ionescu, "Making Sense of Reinforcement Learning and Probabilistic Inference," in *International Conference on Learning Representations*, Sep. 2019.
- [51] I. Osband, J. Aslanides, and A. Cassirer, "Randomized Prior Functions for Deep Reinforcement Learning," in *Advances in Neural Information Processing Systems*, vol. 31. Curran Associates, Inc., 2018.
- [52] D. Hafner, J. Pasukonis, J. Ba, and T. Lillicrap, "Mastering Diverse Domains through World Models," Jan. 2023, arXiv:2301.04104 [cs, stat].
- [53] I. Osband, D. Russo, and B. Van Roy, "(More) Efficient Reinforcement Learning via Posterior Sampling," in *Advances in Neural Information Processing Systems*, vol. 26. Curran Associates, Inc., 2013.
- [54] D. Tiapkin, D. Belomestny, E. Moulines, A. Naumov, S. Samsonov, Y. Tang, M. Valko, and P. Menard, "From Dirichlet to Rubin: Optimistic Exploration in RL without Bonuses," in *Proceedings of the 39th International Conference on Machine Learning*. PMLR, Jun. 2022, pp. 21 380–21 431, iSSN: 2640-3498.
- [55] I. Osband, B. Van Roy, D. J. Russo, and Z. Wen, "Deep Exploration via Randomized Value Functions," *Journal of Machine Learning Research*, vol. 20, pp. 1–62, 2019.
- [56] O. D. Domingues, Y. Flet-Berliac, E. Leurent, P. Ménard, X. Shang, and M. Valko, "rlberry - A Reinforcement Learning Library for Research and Education," Oct. 2021.
- [57] R. Agarwal, M. Schwarzer, P. S. Castro, A. C. Courville, and M. Bellemare, "Deep reinforcement learning at the edge of the statistical precipice," *Advances in Neural Information Processing Systems*, vol. 34, 2021.
- [58] E. Todorov, T. Erez, and Y. Tassa, "Mujoco: A physics engine for model-based control," in *IEEE/RSJ International Conference on Intelligent Robots and systems*. IEEE, 2012, pp. 5026–5033.
- [59] G. An, S. Moon, J.-H. Kim, and H. O. Song, "Uncertainty-Based Offline Reinforcement Learning with Diversified Q-Ensemble," in *Advances in Neural Information Processing Systems*, vol. 34. Curran Associates, Inc., 2021, pp. 7436–7447.
- [60] S. Fujimoto, H. van Hoof, and D. Meger, "Addressing Function Approximation Error in Actor-Critic Methods," in *International Conference on Machine Learning*, ser. Proceedings of Machine Learning Research, J. Dy and A. Krause, Eds., vol. 80. PMLR, Jul. 2018, pp. 1587–1596.
- [61] L. Pineda, B. Amos, A. Zhang, N. O. Lambert, and R. Calandra, "MBRL-Lib: A Modular Library for Model-based Reinforcement Learning," *arXiv:2104.10159 [cs, eess]*, Apr. 2021, arXiv:2104.10159 [cs, eess] type: article.



Carlos E. Luis is a PhD candidate at Bosch Corporate Research and the Intelligent Autonomous Systems group at the Technical University of Darmstadt. Previously, he received a BSc in Electronics Engineering from University Simon Bolivar and a MSc in Aerospace Studies from University of Toronto. Before joining Bosch, he worked as a software development engineer at Amazon. His research is focused in sample-efficient reinforcement learning and uncertainty quantification.



Alessandro G. Bottero is a PhD candidate at Bosch Corporate Research and the Intelligent Autonomous Systems group at the Technical University of Darmstadt. Previously, he received a BSc in Physics from Università degli studi di Pavia and a MSc in Theoretical Physics from Ludwig-Maximilians-Universität of Munich. Before joining Bosch, he worked as a software consultant at TNG - Technology Consulting. His research is focused in safe exploration in Bayesian optimization and reinforcement learning.



Julia Vinogradska is a group leader in black-box optimization methods at Bosch Corporate Research. She received a BSc and MSc degree in mathematics from the University of Stuttgart, and a PhD from the Technical University of Darmstadt. She has received the Stiftung Werner von Siemens Ring Jungwissenschaftler (junior scientist) award for the research conducted during her PhD studies.



Felix Berkenkamp is a lead research scientist and activity lead at Bosch Corporate Research. Previously, he completed a PhD at ETH Zurich, for which he received the ELLIS PhD award. During his PhD studies, he held a AI fellowship from the Open Philanthropy Project, was an Associated Fellow at the Max Planck ETH Center for Learning systems and a postgraduate affiliate at the Vector institute. He served as the workflow co-chair for ICML 2018, publication chair for ICML 2024, and completed research internships at

Microsoft Research and Deepmind. He is interested in the fundamental problems behind data-efficient and safe reinforcement learning with the goal of enabling learning on real-world systems.



Jan Peters is a full professor (W3) for Intelligent Autonomous Systems at the Computer Science Department of the Technische Universität Darmstadt and at the same time a research department head at the German Research Center for Artificial Intelligence (DFKI). He has received a number of awards, including in particular the Dick Volz Best 2007 US Ph.D. Thesis Runner-Up Award, the Robotics: Science & Systems - Early Career Spotlight, the INNS Young Investigator Award, and the IEEE Robotics & Automation Society's

Early Career Award as well as numerous best paper awards. He has received a prestigious ERC Starting Grant and was promoted to a fellow by many well-known research associations (IEEE, AAIA, ELLIS). His PhD students have received prestigious PhD awards including twice the Georges Girault Award for best European Robotics PhD Thesis (and, additionally, two more have been runner-up for that award).

Supplementary Material for “Model-Based Epistemic Variance for Risk-Aware Policy Optimization”

Carlos E. Luis, Alessandro G. Bottero, Julia Vinogradska, Felix Berkenkamp, and Jan Peters

APPENDIX A THEORY PROOFS

A.1 Proof of Theorem 1

In this section, we provide the formal proof of Theorem 1. We begin by showing an expression for the posterior variance of the value function without assumptions on the MDP. We define the joint distribution $p^\pi(a, s' | s) = \pi(a | s)p(s' | s, a)$ for a generic transition function p . To ease notation, since π is fixed, we will simply denote the joint distribution as $p(a, s' | s)$.

Lemma 1. *For any $s \in \mathcal{S}$ and any policy π , it holds that*

$$\mathbb{V}_{p \sim \Phi} [V^{\pi, p}(s)] = \gamma^2 \mathbb{E}_{p \sim \Phi} \left[\left(\sum_{a, s'} p(a, s' | s) V^{\pi, p}(s') \right)^2 \right] - \gamma^2 \left(\mathbb{E}_{p \sim \Phi} \left[\sum_{a, s'} p(a, s' | s) V^{\pi, p}(s') \right] \right)^2. \quad (15)$$

Proof. Using the Bellman expectation equation

$$V^{\pi, p}(s) = \sum_a \pi(a | s) r(s, a) + \gamma \sum_{a, s'} p(a, s' | s) V^{\pi, p}(s'), \quad (16)$$

we have

$$\mathbb{V}_{p \sim \Phi} [V^{\pi, p}(s)] = \mathbb{V}_{p \sim \Phi} \left[\sum_a \pi(a | s) r(s, a) + \gamma \sum_{a, s'} p(a, s' | s) V^{\pi, p}(s') \right] \quad (17)$$

$$= \mathbb{V}_{p \sim \Phi} \left[\gamma \sum_{a, s'} p(a, s' | s) V^{\pi, p}(s') \right], \quad (18)$$

where (18) holds since $r(s, a)$ is deterministic. Using the identity $\mathbb{V}[Y] = \mathbb{E}[Y^2] - (\mathbb{E}[Y])^2$ on (18) concludes the proof. \square

The next result is the direct consequence of our set of assumptions.

Lemma 2. *Under Assumptions 1 and 2, for any $s \in \mathcal{S}$, any policy π , $\text{Cov}[p(s' | s, a), V^{\pi, p}(s')] = 0$.*

Proof. Let $\tau_{0:H}$ be a random trajectory of length $H < |\mathcal{S}|$ steps with the random transition dynamics p . Under Assumption 2, $\tau_{0:H}$ is a sequence of H random, but *unique* states $\{s_0, s_1, \dots, s_{H-1}\}$, i.e., we have $s_i \neq s_j$ for all $i \neq j$. Moreover, under Assumption 1, the conditioned trajectory probability $\mathbb{P}(\tau_{0:H} | p)$, which is itself a random variable through conditioning on p , is a product of independent random variables defined by

$$\mathbb{P}(\tau_{0:H} | p) = \prod_{h=0}^{H-1} \pi(a_h | a_h) p(s_{h+1} | s_h, a_h) \quad (19)$$

$$= p(s_1 | s_0, a_0) \pi(a_0 | a_0) \prod_{h=1}^{H-1} \pi(a_h | s_h) p(s_{h+1} | s_h, a_h). \quad (20)$$

$$= p(s_1 | s_0, a_0) \pi(a_0 | s_0) \mathbb{P}(\tau_{1:H} | p). \quad (21)$$

Note that each transition probability in $\mathbb{P}(\tau_{0:H} | p)$ is distinct by Assumption 2 and there is an implicit assumption that the policy π is independent of p . Then, for arbitrary $s_0 = s, a_0 = a$ and $s_1 = s'$, we have that $p(s' | s, a)$ is independent of $\mathbb{P}(\tau_{1:H} | p)$. Since $V^{\pi, p}(s_1 | s_1 = s')$ is a function of $\mathbb{P}(\tau_{1:H} | p)$, then it is also independent of $p(s' | s, a)$. Finally, since independence implies zero correlation, the lemma holds. \square

Using the previous result yields the following lemma.

Lemma 3. *Under Assumptions 1 and 2, it holds that*

$$\sum_{a, s'} \mathbb{E}_{p \sim \Phi} [p(a, s' | s) V^{\pi, p}(s')] = \sum_{a, s'} \bar{p}(a, s' | s) \mathbb{E}_{p \sim \Phi} [V^{\pi, p}(s')]. \quad (22)$$

Proof. For any pair of random variables X and Y on the same probability space, by definition of covariance it holds that $\mathbb{E}[XY] = \text{Cov}[X, Y] + \mathbb{E}[X] \mathbb{E}[Y]$. Using this identity with Lemma 2 and the definition of posterior mean transition (2) yields the result. \square

Now we are ready to prove the main theorem.

Theorem 1. *Under Assumptions 1 and 2, for any $s \in \mathcal{S}$ and policy π , the posterior variance of the value function, $U^\pi = \mathbb{V}_{p \sim \Phi}[V^{\pi, P}]$ obeys the uncertainty Bellman equation*

$$U^\pi(s) = \gamma^2 u(s) + \gamma^2 \sum_{a, s'} \pi(a | s) \bar{p}(s' | s, a) U^\pi(s'), \quad (6)$$

where $u(s)$ is the local uncertainty defined as

$$u(s) = \mathbb{V}_{a, s' \sim \pi, \bar{p}}[\bar{V}^\pi(s')] - \mathbb{E}_{p \sim \Phi}[\mathbb{V}_{a, s' \sim \pi, p}[V^{\pi, P}(s')]]. \quad (7)$$

Proof. Starting from the result in Lemma 1, we consider each term on the r.h.s of (15) separately. For the first term, notice that within the expectation we have a squared expectation over the transition probability $p(s' | s, a)$, thus using the identity $(\mathbb{E}[Y])^2 = \mathbb{E}[Y^2] - \mathbb{V}[Y]$ results in

$$\mathbb{E}_{p \sim \Phi} \left[\left(\sum_{a, s'} p(a, s' | s) V^{\pi, P}(s') \right)^2 \right] = \mathbb{E}_{p \sim \Phi} \left[\sum_{a, s'} p(a, s' | s) (V^{\pi, P}(s'))^2 - \mathbb{V}_{a, s' \sim \pi, p}[V^{\pi, P}(s')] \right]. \quad (23)$$

Applying linearity of expectation to bring it inside the sum and an application of Lemma 3 (note that the lemma applies for squared values as well) gives

$$= \sum_{a, s'} \bar{p}(a, s' | s) \mathbb{E}_{p \sim \Phi} \left[(V^{\pi, P}(s'))^2 \right] - \mathbb{E}_{p \sim \Phi} \left[\mathbb{V}_{a, s' \sim \pi, p}[V^{\pi, P}(s')] \right]. \quad (24)$$

For the second term of the r.h.s of (15) we apply again Lemma 3 and under definition of variance

$$\left(\mathbb{E}_{p \sim \Phi} \left[\sum_{a, s'} p(a, s' | s) V^{\pi, P}(s') \right] \right)^2 = \left(\sum_{a, s'} \bar{p}(a, s' | s) \mathbb{E}_{p \sim \Phi} [V^{\pi, P}(s')] \right)^2 \quad (25)$$

$$= \sum_{a, s'} \bar{p}(a, s' | s) \left(\mathbb{E}_{p \sim \Phi} [V^{\pi, P}(s')] \right)^2 - \mathbb{V}_{a, s' \sim \pi, \bar{p}} \left[\mathbb{E}_{p \sim \Phi} [V^{\pi, P}(s')] \right]. \quad (26)$$

Finally, since

$$\mathbb{E}_{p \sim \Phi} \left[(V^{\pi, P}(s'))^2 \right] - \left(\mathbb{E}_{p \sim \Phi} [V^{\pi, P}(s')] \right)^2 = \mathbb{V}_{p \sim \Phi} [V^{\pi, P}(s')] \quad (27)$$

for any $s' \in \mathcal{S}$, we can plug (24) and (26) into (15), which proves the theorem. \square

A.2 Proof of Theorem 2

In this section, we provide the supporting theory and the proof of Theorem 2. First, we will use the identity $\mathbb{V}[\mathbb{E}[Y|X]] = \mathbb{E}[(\mathbb{E}[Y|X])^2] - (\mathbb{E}[E[Y|X]])^2$ to prove $u(s) = w(s) - g(s)$ holds, with $Y = \sum_{a, s'} p(a, s' | s) V^{\pi, P}(s')$. For the conditioning variable X , we define a transition function with fixed input state s as a mapping $p_s : \mathcal{A} \rightarrow \Delta(\mathcal{S})$ representing a distribution $p_s(s' | a) = p(s' | s, a)$. Then $X = \mathbf{P}_s := \{p_s(s' | a)\}_{s' \in \mathcal{S}, a \in \mathcal{A}}$. The transition function p_s is drawn from a distribution Φ_s obtained by marginalizing Φ on all transitions not starting from s .

Lemma 4. *Under Assumptions 1 and 2, it holds that*

$$\mathbb{V}_{p_s \sim \Phi_{s, t}} \left[\mathbb{E}_{p \sim \Phi} \left[\sum_{a, s'} p(a, s' | s) V^{\pi, P}(s') \mid \mathbf{P}_s \right] \right] = \mathbb{V}_{p \sim \Phi} \left[\sum_{a, s'} p(a, s' | s) \bar{V}^\pi(s') \right]. \quad (28)$$

Proof. Treating the inner expectation,

$$\mathbb{E}_{p \sim \Phi} \left[\sum_{a, s'} p(a, s' | s) V^{\pi, P}(s') \mid \mathbf{P}_s \right] = \sum_a \pi(a | s) \sum_{s'} \mathbb{E}_{p \sim \Phi} [p(s' | s, a) V^{\pi, P}(s') \mid \mathbf{P}_s]. \quad (29)$$

Due to the conditioning, $p(s' | s, a)$ is deterministic within the expectation

$$= \sum_{a, s'} p(a, s' | s) \mathbb{E}_{p \sim \Phi} [V^{\pi, P}(s') \mid \mathbf{P}_s]. \quad (30)$$

By Lemma 2, $V^{\pi, P}(s')$ is independent of \mathbf{P}_s , so we can drop the conditioning

$$= \sum_{a, s'} p(a, s' | s) \bar{V}^\pi(s'). \quad (31)$$

Lastly, since drawing samples from a marginal distribution is equivalent to drawing samples from the joint, i.e., $\mathbb{V}_x[f(x)] = \mathbb{V}_{(x,y)}[f(x)]$, then:

$$\mathbb{V}_{p_s \sim \Phi_{s,t}} \left[\sum_{a,s'} p(a, s' | s) \bar{V}^\pi(s') \right] = \mathbb{V}_{p \sim \Phi} \left[\sum_{a,s'} p(a, s' | s) \bar{V}^\pi(s') \right], \quad (32)$$

completing the proof. \square

The next lemma establishes the result for the expression $\mathbb{E}[(\mathbb{E}[Y|X])^2]$.

Lemma 5. *Under Assumptions 1 and 2, it holds that*

$$\mathbb{E}_{p_s \sim \Phi_{s,t}} \left[\left(\mathbb{E}_{p \sim \Phi} \left[\sum_{a,s'} p(a, s' | s) V^{\pi,p}(s') \mid \mathbf{P}_s \right] \right)^2 \right] = \sum_{a,s'} \bar{p}(a, s' | s) (\bar{V}^\pi(s')) - \mathbb{E}_{p \sim \Phi} [\mathbb{V}_{a,s' \sim \pi,p} [\bar{V}^\pi(s')]]. \quad (33)$$

Proof. The inner expectation is equal to the one in Lemma 4, so we have that

$$\left(\mathbb{E}_{p \sim \Phi} \left[\sum_{a,s'} p(a, s' | s) V^{\pi,p}(s') \mid \mathbf{P}_s \right] \right)^2 = \left(\sum_{a,s'} p(a, s' | s) \bar{V}^\pi(s') \right)^2 \quad (34)$$

$$= \sum_{a,s'} p(a, s' | s) (\bar{V}^\pi(s'))^2 - \mathbb{V}_{a,s' \sim \pi,p} [\bar{V}^\pi(s')]. \quad (35)$$

Finally, applying expectation on both sides of (35) yields the result. \square

Similarly, the next lemma establishes the result for the expression $(\mathbb{E}[\mathbb{E}[Y|X]])^2$.

Lemma 6. *Under Assumptions 1 and 2, it holds that*

$$\left(\mathbb{E}_{p_s \sim \Phi_{s,t}} \left[\mathbb{E}_{p \sim \Phi} \left[\sum_{a,s'} p(a, s' | s) V^{\pi,p}(s') \mid \mathbf{P}_s \right] \right] \right)^2 = \sum_{a,s'} \bar{p}(a, s' | s) (\bar{V}^\pi(s')) - \mathbb{V}_{a,s' \sim \pi,\bar{p}} [\bar{V}^\pi(s')]. \quad (36)$$

Proof. By the tower property of expectations, $(\mathbb{E}[\mathbb{E}[Y|X]])^2 = (\mathbb{E}[Y])^2$. Then, the result follows directly from (25) and (26). \square

The second part of Theorem 2 is a corollary of the next lemma.

Lemma 7. *Under Assumptions 1 and 2, it holds that*

$$\mathbb{E}_{p \sim \Phi} [\mathbb{V}_{a,s' \sim \pi,p} [V^{\pi,p}(s')] - \mathbb{V}_{a,s' \sim \pi,p} [\bar{V}^\pi(s')]] \quad (37)$$

is non-negative.

Proof. We will prove the lemma by showing (37) is equal to $\mathbb{E}_{p \sim \Phi} [\mathbb{V}_{a,s' \sim \pi,p} [V^{\pi,p}(s') - \bar{V}^\pi(s')]]$, which is a non-negative quantity by definition of variance. The idea is to derive two expressions for $\mathbb{E}[\mathbb{V}[Y|X]]$ and compare them. First, we will use the identity $\mathbb{E}[\mathbb{V}[Y|X]] = \mathbb{E}[\mathbb{E}[(Y - \mathbb{E}[Y|X])^2|X]]$. The outer expectation is w.r.t the marginal distribution Φ_s while the inner expectations are w.r.t Φ . For the inner expectation we have

$$\mathbb{E}_{p \sim \Phi} \left[\left(\sum_{a,s'} p(a, s' | s) V^{\pi,p}(s') - \mathbb{E}_{p \sim \Phi} \left[\sum_{a,s'} p(a, s' | s) V^{\pi,p}(s') \mid \mathbf{P}_s \right] \right)^2 \mid \mathbf{P}_s \right] \quad (38)$$

$$= \mathbb{E}_{p \sim \Phi} \left[\left(\sum_{a,s'} p(a, s' | s) (V^{\pi,p}(s') - \mathbb{E}_{p \sim \Phi} [V^{\pi,p} \mid \mathbf{P}_s]) \right)^2 \mid \mathbf{P}_s \right] \quad (39)$$

$$= \mathbb{E}_{p \sim \Phi} \left[\left(\sum_{a,s'} p(a, s' | s) (V^{\pi,p}(s') - \bar{V}^\pi(s')) \right)^2 \mid \mathbf{P}_s \right] \quad (40)$$

$$= \mathbb{E}_{p \sim \Phi} \left[\sum_{a,s'} p(a, s' | s) (V^{\pi,p}(s') - \bar{V}^\pi(s'))^2 - \mathbb{V}_{a,s' \sim \pi,p} [V^{\pi,p}(s') - \bar{V}^\pi(s')] \mid \mathbf{P}_s \right] \quad (41)$$

$$= \sum_{a,s'} p(a, s' | s) \mathbb{V}_{p \sim \Phi} [V^{\pi,p}(s')] - \mathbb{E}_{p \sim \Phi} [\mathbb{V}_{a,s' \sim \pi,p} [V^{\pi,p}(s') - \bar{V}^\pi(s')] \mid \mathbf{P}_s]. \quad (42)$$

Applying the outer expectation to the last equation, along with Lemma 2 and the tower property of expectations yields:

$$\mathbb{E}[\mathbb{V}[Y|X]] = \sum_{a,s'} \bar{p}(a, s' | s) \mathbb{V}_{p \sim \Phi} [V^{\pi,p}(s')] - \mathbb{E}_{p \sim \Phi} [\mathbb{V}_{a,s' \sim \pi,p} [V^{\pi,p}(s') - \bar{V}^\pi(s')]]. \quad (43)$$

Now we repeat the derivation but using $\mathbb{E}[\mathbb{V}[Y|X]] = \mathbb{E}[\mathbb{E}[Y^2|X] - (\mathbb{E}[Y|X])^2]$. For the inner expectation of the first term we have:

$$\mathbb{E}_{p \sim \Phi} \left[\left(\sum_{a,s'} p(a, s' | s) V^{\pi,p}(s') \right)^2 \middle| \mathbf{P}_s \right] \quad (44)$$

$$= \mathbb{E}_{p \sim \Phi} \left[\sum_{a,s'} p(a, s' | s) (V^{\pi,p}(s'))^2 - \mathbb{V}_{a,s' \sim \pi,p} [V^{\pi,p}(s')] \middle| \mathbf{P}_s \right]. \quad (45)$$

Applying the outer expectation:

$$\mathbb{E}[\mathbb{E}[Y^2|X]] = \sum_{a,s'} \bar{p}(a, s' | s) \mathbb{E}_{p \sim \Phi} [(V^{\pi,p}(s'))^2] - \mathbb{E}_{p \sim \Phi} [\mathbb{V}_{a,s' \sim \pi,p} [V^{\pi,p}(s')]]. \quad (46)$$

Lastly, for the inner expectation of $\mathbb{E}[(\mathbb{E}[Y|X])^2]$:

$$\left(\mathbb{E}_{p \sim \Phi} \left[\sum_{a,s'} p(a, s' | s) V^{\pi,p}(s') \middle| \mathbf{P}_s \right] \right)^2 = \left(\sum_{a,s'} p(a, s' | s) \bar{V}^\pi(s') \right)^2 \quad (47)$$

$$= \sum_{a,s'} p(a, s' | s) (\bar{V}^\pi(s'))^2 - \mathbb{V}_{a,s' \sim \pi,p} [\bar{V}^\pi(s')]. \quad (48)$$

Applying the outer expectation:

$$\mathbb{E}[(\mathbb{E}[Y|X])^2] = \sum_{a,s'} \bar{p}(a, s' | s) (\bar{V}^\pi(s'))^2 - \mathbb{E}_{p \sim \Phi} [\mathbb{V}_{a,s' \sim \pi,p} [\bar{V}^\pi(s')]]. \quad (49)$$

Finally, by properties of variance, (43) = (46) - (49) which gives the desired result. \square

Theorem 2. Under Assumptions 1 and 2, for any $s \in \mathcal{S}$ and policy π , it holds that $u(s) = w(s) - g(s)$, where $g(s) = \mathbb{E}_{p \sim \Phi} [\mathbb{V}_{a,s' \sim \pi,p} [V^{\pi,p}(s')] - \mathbb{V}_{a,s' \sim \pi,p} [\bar{V}^\pi(s')]]$. Furthermore, we have that the gap $g(s)$ is non-negative, thus $u(s) \leq w(s)$.

Proof. By definition of $u(s)$ in (7), proving the claim is equivalent to showing

$$\mathbb{V}_{a,s' \sim \pi, \bar{p}} [\bar{V}^\pi(s')] = w(s) + \mathbb{E}_{p \sim \Phi} [\mathbb{V}_{a,s' \sim \pi,p} [\bar{V}^\pi(s')]], \quad (50)$$

which holds by combining Lemmas 4–6. Lastly, $u(s) \leq w(s)$ holds by Lemma 7. \square

APPENDIX B THEORY EXTENSIONS

B.1 Unknown Reward Function

We can easily extend the derivations on Appendix A.1 to include the additional uncertainty coming from an *unknown* reward function. Similarly, we assume the reward function is a random variable r drawn from a prior distribution $\Psi(r)$, and whose belief will be updated via Bayes rule. In this new setting, we now consider the variance of the values under the distribution of MDPs, represented by the random variable \mathcal{M} . We need the following additional assumptions to extend our theory.

Assumption 3 (Independent rewards). $r(x, a)$ and $r(y, a)$ are independent random variables if $x \neq y$.

Assumption 4 (Independent transitions and rewards). The random variables $p(\cdot | s, a)$ and $r(s, a)$ are independent for any (s, a) .

With Assumption 3 we have that the value function of next states is independent of the transition function and reward function at the current state. Assumption 4 means that sampling $\mathcal{M} \sim \Gamma$ is equivalent as independently sampling $p \sim \Phi$ and $r \sim \Psi$.

Theorem 3. Under Assumptions 1–4, for any $s \in \mathcal{S}$ and policy π , the posterior variance of the value function, $U^\pi = \mathbb{V}_{\mathcal{M} \sim \Gamma} [V^{\pi, \mathcal{M}}]$ obeys the uncertainty Bellman equation

$$U^\pi(s) = \mathbb{V}_{r \sim \Psi} \left[\sum_a \pi(a | s) r(s, a) \right] + \gamma^2 u(s) + \gamma^2 \sum_{a,s'} \pi(a | s) \bar{p}(s' | s, a) U^\pi(s'), \quad (51)$$

where $u(s)$ is defined in (7).

Proof. By Assumptions 3 and 4 and following the derivation of Lemma 1 we have

$$\mathbb{V}_{\mathcal{M} \sim \Gamma} [V^{\pi, \mathcal{M}}(s)] = \mathbb{V}_{\mathcal{M} \sim \Gamma} \left[\sum_a \pi(a | s) r(s, a) + \gamma \sum_{a, s'} p(a, s' | s) V^{\pi, \mathcal{M}}(s') \right] \quad (52)$$

$$= \mathbb{V}_{r \sim \Psi} \left[\sum_a \pi(a | s) r(s, a) \right] + \mathbb{V}_{\mathcal{M} \sim \Gamma} \left[\gamma \sum_{a, s'} p(a, s' | s) V^{\pi, \mathcal{M}}(s') \right]. \quad (53)$$

Then following the same derivations as Appendix A.1 completes the proof. \square

B.2 Extension to Q -values

Our theoretical results naturally extend to action-value functions. The following result is analogous to Theorem 1.

Theorem 4. Under Assumptions 1 and 2, for any $(s, a) \in \mathcal{S} \times \mathcal{A}$ and policy π , the posterior variance of the Q -function, $U^\pi = \mathbb{V}_{p \sim \Phi} [Q^{\pi, p}]$ obeys the uncertainty Bellman equation

$$U^\pi(s, a) = \gamma^2 u(s, a) + \gamma^2 \sum_{a', s'} \pi(a' | s') \bar{p}(s' | s, a) U^\pi(s', a'), \quad (54)$$

where $u(s, a)$ is the local uncertainty defined as

$$u(s, a) = \mathbb{V}_{a', s' \sim \pi, \bar{p}} [\bar{Q}^\pi(s', a')] - \mathbb{E}_{p \sim \Phi} [\mathbb{V}_{a', s' \sim \pi, p} [Q^{\pi, p}(s', a')]] \quad (55)$$

Proof. Follows the same derivation as Appendix A.1 \square

Similarly, we can connect to the upper-bound found by [11] with the following theorem.

Theorem 5. Under Assumptions 1 and 2, for any $(s, a) \in \mathcal{S} \times \mathcal{A}$ and policy π , it holds that $u(s, a) = w(s, a) - g(s, a)$, where $w(s, a) = \mathbb{V}_{p \sim \Phi} [\sum_{a', s'} \pi(a' | s') p(s' | s, a) \bar{Q}^\pi(s', a')]$ and $g(s, a) = \mathbb{E}_{p \sim \Phi} [\mathbb{V}_{a', s' \sim \pi, p} [Q^{\pi, p}(s', a')]] - \mathbb{V}_{a', s' \sim \pi, p} [\bar{Q}^\pi(s', a')]$. Furthermore, we have that the gap $g(s, a) \geq 0$ is non-negative, thus $u(s, a) \leq w(s, a)$.

Proof. Follows the same derivation as Appendix A.2. Similarly, we can prove that the gap $g(s, a)$ is non-negative by showing it is equal to $\mathbb{E}_{p \sim \Phi} [\mathbb{V}_{a', s' \sim \pi, p} [Q^{\pi, p}(s', a') - \bar{Q}^\pi(s', a')]]$. \square

B.3 State-Action Uncertainty Rewards

In our practical experiments, we use the results of both Appendices B.1 and B.2 to compose the uncertainty rewards propagated via the UBE. Concretely, we consider the following two approaches for computing state-action uncertainty rewards:

- pombu:

$$w(s, a) = \mathbb{V}_{p \sim \Phi} \left[\sum_{a', s'} \pi(a' | s') p(s' | s, a) \bar{Q}^\pi(s', a') \right] \quad (56)$$

- exact-ube:

$$u(s, a) = w(s, a) - \mathbb{E}_{p \sim \Phi} [\mathbb{V}_{a', s' \sim \pi, p} [Q^{\pi, p}(s', a') - \bar{Q}^\pi(s', a')]] \quad (57)$$

Additionally, since we also learn the reward function, we add to the above the uncertainty term generated by the reward function posterior, as shown in Appendix B.1: $\mathbb{V}_{r \sim \Psi} [r(s, a)]$.

APPENDIX C

TABULAR ENVIRONMENTS EXPERIMENTS

In this section, we provide more details about the tabular implementation of Algorithm 1, environment details and extended results.

C.1 Implementation Details

Model learning. For the transition function we use a prior $\text{Dirichlet}(1/\sqrt{S})$ and for rewards a standard normal $\mathcal{N}(0, 1)$, as done by [50]. The choice of priors leads to closed-form posterior updates based on state-visitation counts and accumulated rewards. We add a terminal state to our modeled MDP in order to compute the values in closed-form via linear algebra.

Accelerating learning. For the *DeepSea* benchmark we accelerate learning by imagining each experienced transition (s, a, s', r) is repeated L times, as initially suggested in [55] (see footnote 9), although we scale the number of repeats with the size of the MDP. Effectively, this strategy forces the MDP posterior to shrink faster, thus making all algorithms converge in fewer episodes. The same strategy was used for all the methods evaluated in the benchmark.

Policy optimization. All tested algorithms (PSRL and OFU variants) optimize the policy via policy iteration, where we break ties at random when computing the argmax, and limit the number of policy iteration steps to 40.

Hyperparameters. Unless noted otherwise, all tabular RL experiments use a discount factor $\gamma = 0.99$, an exploration gain $\lambda = 1.0$ and an ensemble size $N = 5$.

Uncertainty reward clipping. For *DeepSea* we clip uncertainty rewards with $u_{\min} = -0.05$ and for the 7-room environment we keep $u_{\min} = 0.0$.

C.2 Environment Details

DeepSea. As proposed by [55], *DeepSea* is a grid-world environment of size $L \times L$, with $S = L^2$ and $A = 2$.

7-room. As implemented by [56], the 7-room environment consists of seven connected rooms of size 5×5 , represented as an MDP of size $S = 181$ and discrete action space with size $A = 4$. The starting state is always the center cell of the middle room, which yields a reward of 0.01. The center cell of the left-most room gives a reward of 0.1 and the center cell of the right-most room gives a large reward of 1. The episode terminates after 40 steps and the state with large reward is absorbing (i.e., once it reaches the rewarding state, the agent remains there until the end of the episode). The agent transitions according to the selected action with probability 0.95 and moves to a randomly selected neighboring cell with probability 0.05.

C.3 DeepSea Additional Experiments

C.3.1 Extended Results

Figure 8 shows the total regret in intervals of 50 episodes for all the different *DeepSea* sizes considered. Our method consistently achieves the lowest total regret.

C.3.2 Uncertainty Rewards Ablation

Our theory prescribes equivalent expressions for the uncertainty rewards under the assumptions. However, since it practice the assumptions do not generally hold, the expressions are no longer equivalent. In this section we evaluate the performance in the *DeepSea* benchmark for these different definitions of the uncertainty rewards:

- `exact-ube_1`:

$$u(s, a) = \mathbb{V}_{a', s' \sim \pi, p} [\bar{Q}^\pi(s', a')] - \mathbb{E}_{p \sim \Phi} \left[\mathbb{V}_{a', s' \sim \pi, p} [Q^{\pi, p}(s', a')] \right]$$

- `exact-ube_2`:

$$u(s, a) = \mathbb{V}_{p \sim \Phi} \left[\sum_{a', s'} \pi(a' | s') p(s' | s, a) \bar{Q}^\pi(s', a') \right] - \mathbb{E}_{p \sim \Phi} \left[\mathbb{V}_{a', s' \sim \pi, p} [Q^{\pi, p}(s', a')] - \mathbb{V}_{a', s' \sim \pi, p} [\bar{Q}^\pi(s', a')] \right]$$

- `exact-ube_3` (labeled `exact-ube` in all other plots):

$$u(s, a) = \mathbb{V}_{p \sim \Phi} \left[\sum_{a', s'} \pi(a' | s') p(s' | s, a) \bar{Q}^\pi(s', a') \right] - \mathbb{E}_{p \sim \Phi} \left[\mathbb{V}_{a', s' \sim \pi, p} [Q^{\pi, p}(s', a') - \bar{Q}^\pi(s', a')] \right]$$

Recall that, since we consider an unknown reward function, we add the uncertainty about rewards to the above when solving the UBE. Figure 9 shows the results for the *DeepSea* benchmark comparing the three uncertainty signals. Since the assumptions are violated in the practical setting, the three signals are no longer equivalent and result in slightly different uncertainty rewards. Still, when integrated into Algorithm 1, the performance in terms of learning time and total regret is quite similar. We select `exact-ube_3` as the default estimate for all other experiments.

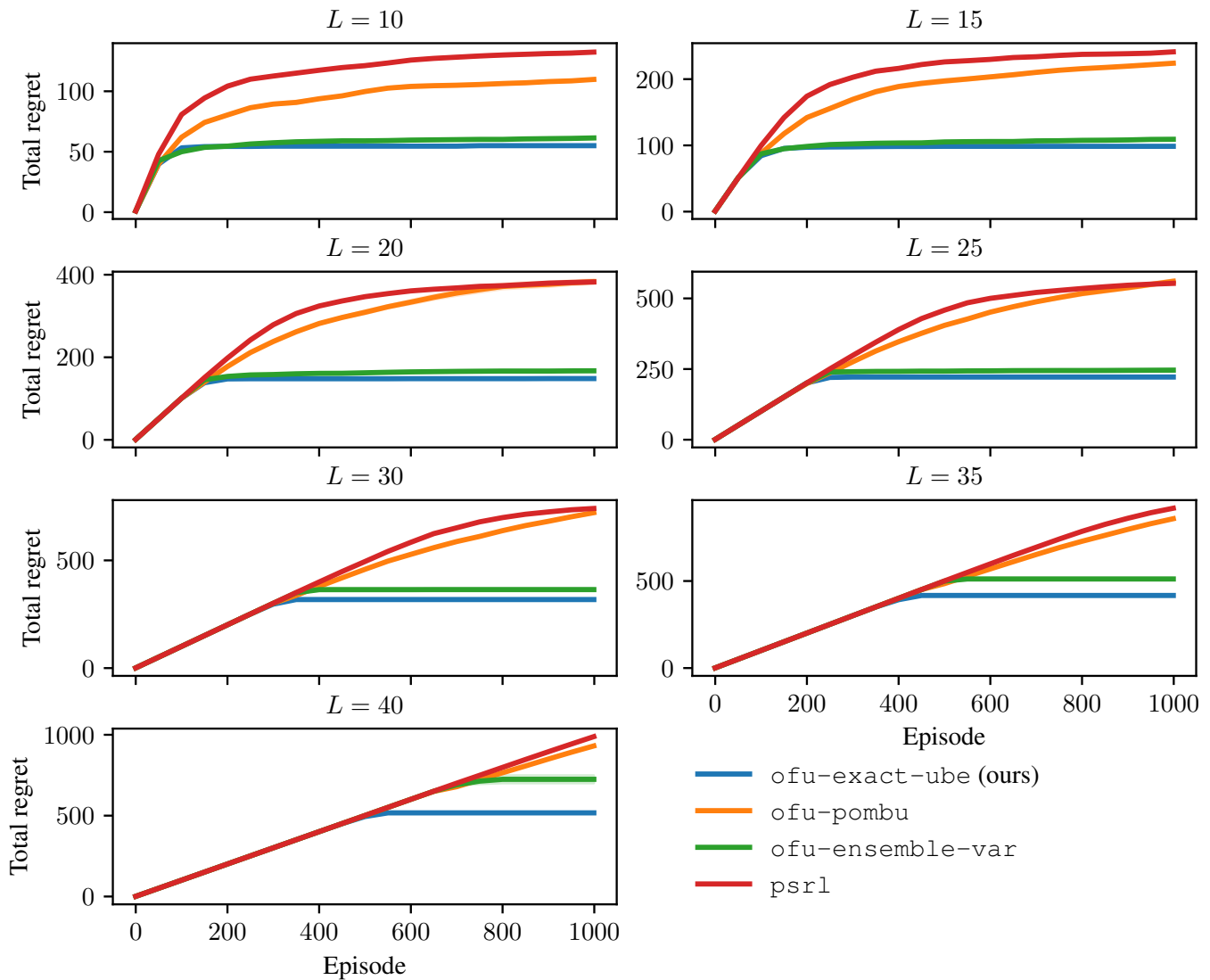


Fig. 8: Extended results for the *DeepSea* experiments shown in Figure 4. We report the average (solid line) and standard error (shaded region) over 5 random seeds.

C.3.3 Ensemble Size Ablation

The ensemble size N is one important hyperparameter for all the OFU-based methods. We perform additional experiments in *DeepSea* for different values of N , keeping all other hyperparameters fixed and with sizes $L = \{20, 30\}$. The results in Figure 10 show that our method achieves lower total regret across the different ensemble sizes. For *ensemble-var*, performance increases for larger ensembles. These results suggest that the sample-based approximation of our uncertainty rewards is not very sensitive to the number of samples and achieve good performance even for $N = 2$.

C.3.4 Exploration Gain Ablation

Another important hyperparameter for OFU-based methods is the exploration gain λ , controlling the magnitude of the optimistic values optimized via policy iteration. We perform an ablation study over λ , keeping all other hyperparameters fixed and testing for *DeepSea* sizes $L = \{20, 30\}$. Figure 11 shows the total regret for OFU methods over increasing gain. Unsurprisingly, as we increase λ , the total regret of all the methods increases, but overall *exact-ube* achieves the best performance.

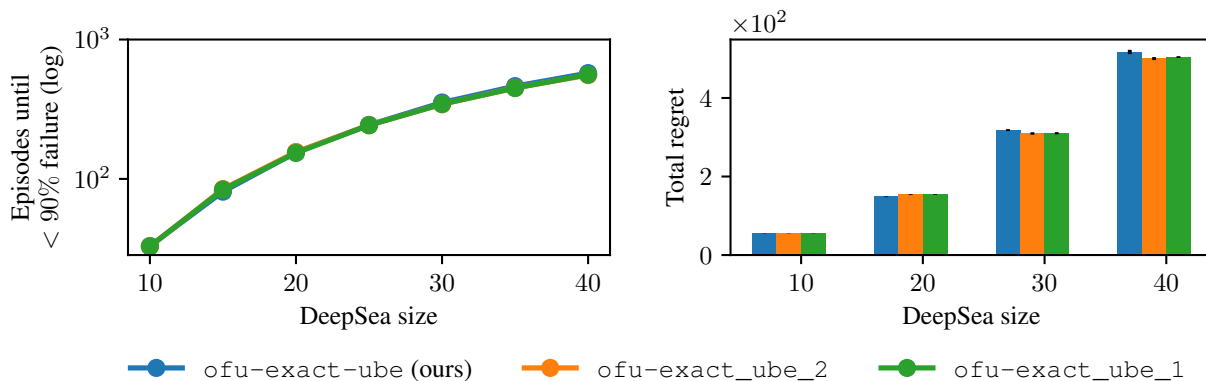


Fig. 9: Ablation study on *DeepSea* exploration for different estimates of *exact-ube*. Results represent the average over 5 random seeds, and vertical bars on total regret indicate the standard error.

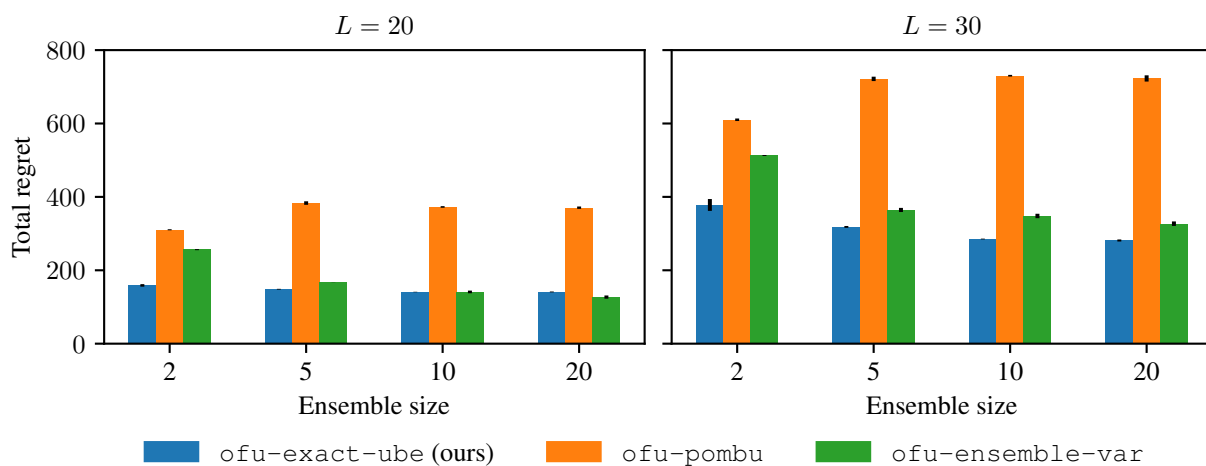


Fig. 10: Ablation study over ensemble size N on the *DeepSea* environment.

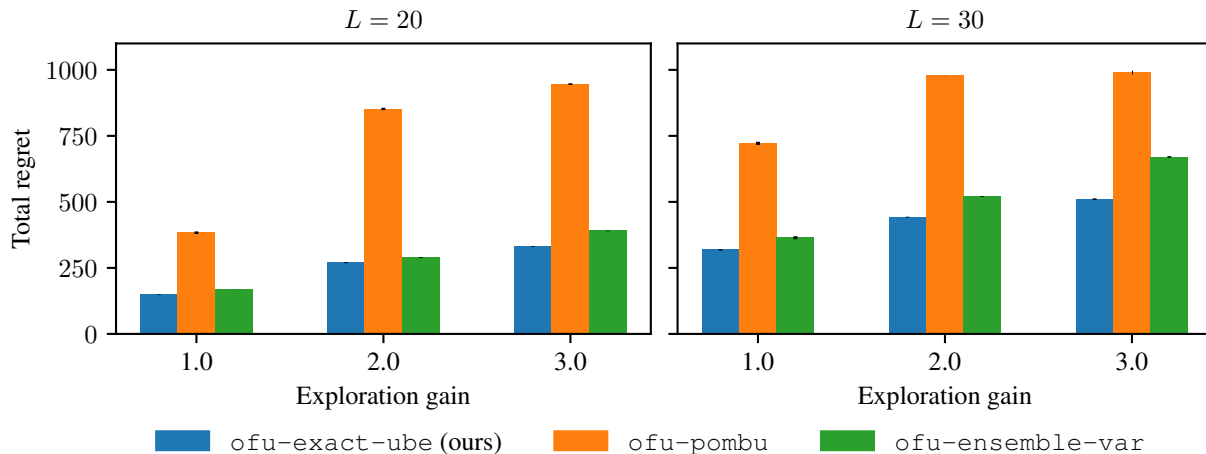


Fig. 11: Ablation study over exploration gain λ on the *DeepSea* environment.

APPENDIX D ONLINE DEEP RL EXPERIMENTS

In this section, we provide details regarding the online implementation of QU-SAC. Also, we include relevant hyperparameters, environment details and additional results.

Algorithm 2 QU-SAC (online)

```

1: Initialize policy  $\pi_\phi$ , predictive model  $p_\theta$ , critic ensemble  $\{Q_i\}_{i=1}^N$ , uncertainty net  $U_\psi$  (optional), environment dataset  $\mathcal{D}$ ,
   model datasets  $\mathcal{D}_{\text{model}}$  and  $\{\mathcal{D}_i\}_{i=1}^N$ .
2: global step  $\leftarrow 0$ 
3: for episode  $t = 0, \dots, T - 1$  do
4:   for  $E$  steps do
5:     if global step %  $F == 0$  then
6:       Train model  $p_\theta$  on  $\mathcal{D}$  via maximum likelihood
7:       for  $M$  model rollouts do
8:         Perform  $k$ -step model rollouts starting from  $s \sim \mathcal{D}$ ; add to  $\mathcal{D}_{\text{model}}$  and  $\{\mathcal{D}_i\}_{i=1}^N$ 
9:       Take action in environment according to  $\pi_\phi$ ; add to  $\mathcal{D}$ 
10:      for  $G$  gradient updates do
11:        Update  $\{Q_i\}_{i=1}^N$  with mini-batches from  $\{\mathcal{D}_i\}_{i=1}^N$ , via SGD on (10)
12:        (Optional) Update  $U_\psi$  with mini-batches from  $\mathcal{D}_{\text{model}}$ , via SGD on (13)
13:        Update  $\pi_\phi$  with mini-batches from  $\mathcal{D}_{\text{model}}$ , via SGD on (14)
14:      global step  $\leftarrow$  global step + 1

```

TABLE 3: Hyperparameters for the DeepMind Control Suite experiments of Section 5.3. For MBPO, the only deviation from the listed parameters is the use of $M = 2$ as the original method uses clipped Q-learning.

Name	Value
General	
T - # episodes	500
E - steps per episode	10^3
Replay buffer \mathcal{D} capacity	10^5
Batch size (all nets)	256
Warm-up steps (under initial policy)	5×10^3
SAC	
G - # gradient steps	10
Auto-tuning of entropy coefficient α ?	Yes
Target entropy	$-\dim(\mathcal{A})$
Actor MLP network	2 hidden layers - 128 neurons - Tanh activations
Critic MLP network	2 hidden layers - 256 neurons - Tanh activations
Actor/Critic learning rate	3×10^{-4}
Dynamics Model	
N - ensemble size	5
F - frequency of model training (# steps)	250
L - # model rollouts per step	400
k - rollout length	5
Δ - # Model updates to retain data	1
Model buffer(s) capacity	$L \times F \times k \times \Delta = 5 \times 10^5$
Model MLP network	4 layers - 200 neurons - SiLU activations
Learning rate	1×10^{-3}
QU-SAC Specific	
M - # critics per dynamics model	1
λ - # uncertainty gain	1.0
Uncertainty type	{ensemble-var, upper-bound}

D.1 Implementation Details

We build QU-SAC on top of MBPO [5] following Algorithm 2. The main differences with the original implementation are as follows:

- In Line 8, we perform a total of $N + 1$ k -step rollouts corresponding to both the model-randomized and model-consistent rollout modalities. The original MBPO only executes the former to fill up $\mathcal{D}_{\text{model}}$.
- In Line 11, we update the ensemble of Q -functions on the corresponding model-consistent buffer. MBPO trains twin critics (as in SAC) on mini-batches from $\mathcal{D}_{\text{model}}$.
- In Line 12, we update the U -net for the UBE-based variance estimation methods.
- In Line 13, we update π_ϕ by maximizing the uncertainty-aware Q -values. MBPO maximizes the minimum of the twin critics (as in SAC). Both approaches include an entropy maximization term.

The main hyperparameters for our experiments are included in Table 3. Further implementation details are now provided.

Model learning. We leverage the `mbrl-lib` Python library from [61] and train an ensemble of N probabilistic neural networks. We use the default MLP architecture with four layers of size 200 and SiLU activations. The networks predict delta

Algorithm 3 QU-SAC (offline)

-
- 1: Initialize policy π_ϕ , predictive model p_θ , critic ensemble $\{Q_i\}_{i=1}^N$, uncertainty net U_ψ (optional), offline dataset \mathcal{D} , model datasets $\mathcal{D}_{\text{model}}$ and $\{\mathcal{D}_i\}_{i=1}^N$.
 - 2: Train model p_θ on \mathcal{D} via maximum likelihood
 - 3: **for** steps $g = 0, \dots, G - 1$ **do**
 - 4: **if** $g \% F == 0$ **then**
 - 5: **for** L model rollouts **do**
 - 6: Perform k -step model rollouts starting from $s \sim \mathcal{D}$; add to $\mathcal{D}_{\text{model}}$ and $\{\mathcal{D}_i\}_{i=1}^N$
 - 7: Update $\{Q_i\}_{i=1}^N$ with mini-batches from $\{\mathcal{D} \cup \mathcal{D}_i\}_{i=1}^N$, via SGD on (10)
 - 8: (Optional) Update U_ψ with mini-batches from $\mathcal{D} \cup \mathcal{D}_{\text{model}}$, via SGD on (13)
 - 9: Update π_ϕ with mini-batches from $\mathcal{D} \cup \mathcal{D}_{\text{model}}$, via SGD on (14)
-

states, $\Delta = s' - s$, and receive as input state-action pairs. We use the default initialization of the network provided by the library, which samples weights from a truncated Gaussian distribution, however we found it helpful to increase by a factor of 2.0 the standard deviation of the truncated Gaussian; a wider distribution of weights allows for more diverse dynamic models at the beginning of training.

Model-generated buffers. The capacity of the model-generated buffers $\mathcal{D}_{\text{model}}$ and $\{\mathcal{D}_{\text{model}}^i\}_{i=1}^N$ is computed as $k \times M \times F \times \Delta$, where Δ is the number of model updates before entirely overwriting the buffers. Larger values of this parameter allows for more off-policy (old) data to be stored and sampled for training.

SAC specifics. Our SAC implementation is based on the open-source repository <https://github.com/pranz24/pytorch-soft-actor-critic>, as done by `mbrl-lib`. For all our experiments, we use the automatic entropy tuning flag that adaptively modifies the entropy gain α based on the stochasticity of the policy.

E.2 Environment Details

We take a subset of sparse reward environments from the DeepMind Control Suite and include an additional action cost proportional to the squared norm of the action taken by the agent. Namely,

$$\text{action_cost} = \rho \sum_{i=1}^{|\mathcal{A}|} a_i^2 \quad (58)$$

where ρ is an environment specific multiplier, a_i is the i -th component of the action vector and $|\mathcal{A}|$ is the size of the action space. For `acrobot`, `reacher-hard` and `cartpole-swingup` we use $\rho = 0.01$; for `pendulum` and `point-mass` we use $\rho = 0.05$; and lastly, for `ball-in-cup` we use $\rho = 0.2$.

APPENDIX E

OFFLINE DEEP RL EXPERIMENTS

In this section, we provide further details regarding the use of QU-SAC for offline optimization, which includes a detailed algorithmic description, hyperparameters and learning curves not included in the main body of the paper.

E.1 Implementation Details

We modify the online version of QU-SAC described in Algorithm 2 to reflect the execution flow of offline optimization, which we present in Algorithm 3. The hyperparameters used for the reported results are included in Table 4. Beyond the algorithmic changes, we now list the main implementation details differing from the online implementation of QU-SAC:

Model learning. The only difference w.r.t. the online setting is that we normalize the state-action inputs to the model, where the normalization statistics are calculated based on the offline dataset \mathcal{D} .

Data mixing. In Lines 7-9, we highlight that, in contrast to the online setting, the mini-batches used to train the critic, actor and U -net mix both model-generated and offline data. In particular, we use a fixed 50/50 split between these two data sources for all our experiments (including QU-SAC and MOPO).

MOPO details. In order to conduct a fair comparison between MOPO and QU-SAC, we implement MOPO in our codebase so that it shares the same core components as our QU-SAC implementation. After initial testing of our MOPO implementation, we found that using an uncertainty penalty of $\lambda = 1.0$ worked well across datasets. Note that our implementation of MOPO (labeled MOPO* in Table 2) significantly outperforms the scores reported by [37], which were obtained by running the original codebase by [12] but on the v2 datasets from D4RL.

E.2 Dataset Details

We use the v2 version of D4RL datasets and evaluate using the normalized scores provided by the software package.

TABLE 4: Hyperparameters for the D4RL experiments of Section 5.4.

Name	Value
General	
G - gradient steps	10^6
Replay buffer \mathcal{D} capacity	10^6
Batch size (all nets)	512
SAC	
Auto-tuning of entropy coefficient α ?	Yes
Target entropy	$-\dim(\mathcal{A})$
Actor MLP network	3 hidden layers - 256 neurons - Tanh activations
Critic MLP network	3 hidden layers - 256 neurons - Tanh activations
Actor learning rate	3×10^{-5}
Critic learning rate	3×10^{-4}
Dynamics Model	
N - ensemble size	5
F - frequency of data collection (# steps)	1000
L - rollout batch size	5×10^4
k - rollout length	15
Δ - # Data collection calls to retain data	5
Model buffer(s) capacity	$L \times k \times \Delta = 3.75 \times 10^6$
Model MLP network	4 layers - 200 neurons - SiLU activations
Learning rate	1×10^{-3}
QU-SAC Specific	
M - # critics per dynamics model	{1, 2}
λ - # uncertainty gain	-1.0
Uncertainty type	{ensemble-var, upper-bound}

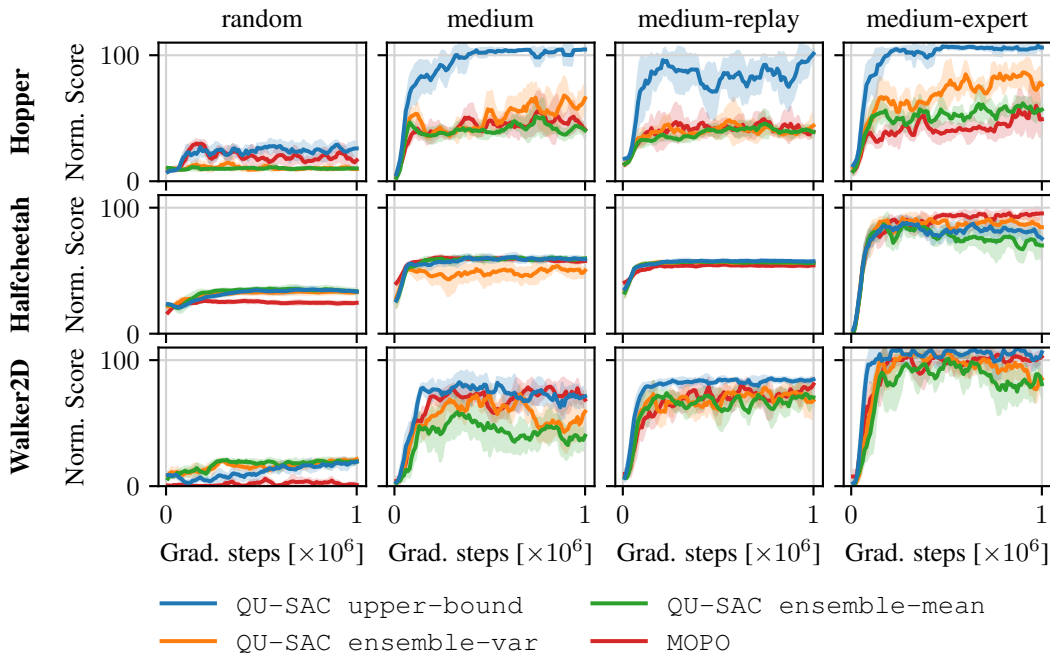


Fig. 12: D4RL smoothed learning curves for $M = 1$. We report the mean and standard deviation over five random seeds of the average normalized score over 10 evaluation episodes.

E.3 D4RL Learning Curves & Scores

In Figures 12 and 13 we include all the learning curves for $M = \{1, 2\}$, respectively. For each run, we report the average normalized score over 10 evaluation episodes. These averaged scores are then also averaged over five independent random seeds to obtain the reported learning curves. In Table 5 we report the associated final scores after 1M gradient steps.

We observe that for $M = 2$ `upper-bound` has lower overall performance than `ensemble-var`. We believe this difference in performance is largely due to using a fixed value of $\lambda = -1.0$ for all experiments. Since using $M = 2$ already acts as a strong regularizer in the offline setting, `upper-bound` would likely benefit from using a lower magnitude λ given the (empirically) larger uncertainty estimates compared to `ensemble-var`.

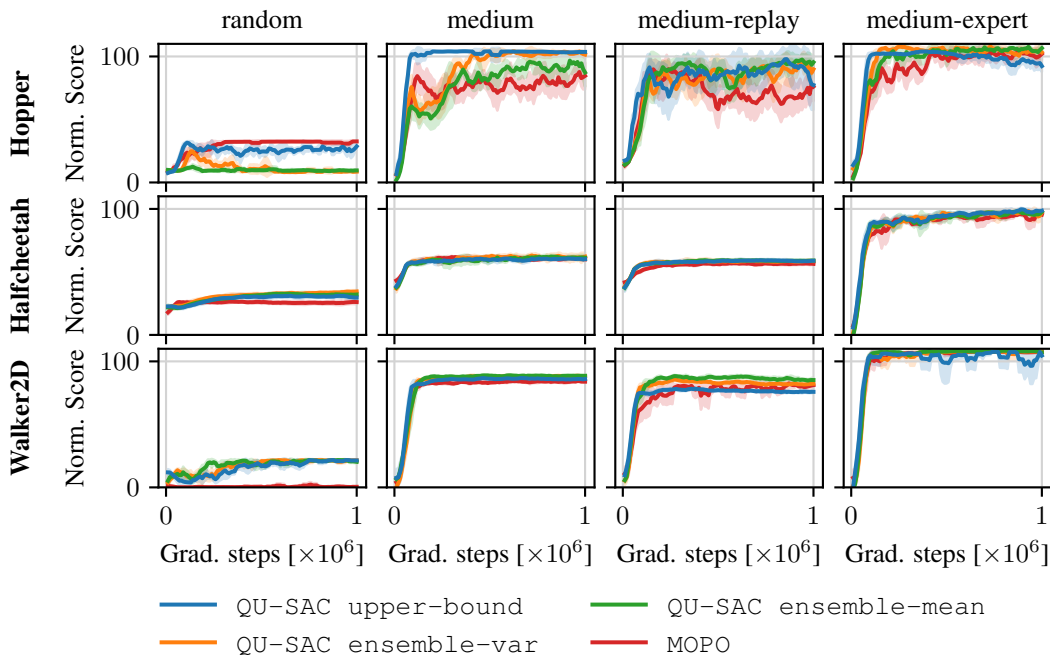


Fig. 13: D4RL smoothed learning curves for $M = 2$. We report the mean and standard deviation over five random seeds of the average normalized score over 10 evaluation episodes.

TABLE 5: D4RL scores after 1M gradient steps. We report the mean and standard deviation over five random seeds of the average normalized score across 10 evaluation episodes. We highlight the highest mean scores for each value of M .

		$M = 1$				$M = 2$			
		MOPO*	e-mean	e-var	u-bound	MOPO*	e-mean	e-var	u-bound
Random	HalfCheetah	24.8±0.7	33.6 ±3.8	33.0±1.7	33.4±1.2	25.9±1.4	32.4±1.8	34.8 ±1.0	30.2±1.5
	Hopper	20.7±9.2	10.3±0.8	9.3±1.8	28.3 ±8.3	32.6 ±0.2	9.8±1.1	8.7±0.8	31.5±0.2
	Walker2D	0.5±0.3	20.3±4.4	21.9 ±1.0	18.2±5.0	1.0±1.9	20.5±2.3	21.7 ±0.1	21.7 ±0.1
Medium	HalfCheetah	57.7±1.5	60.6 ±1.4	58.5±2.9	59.7±2.5	60.6±2.4	60.3±0.8	63.7 ±2.3	60.6±1.7
	Hopper	35.4±4.1	41.4±8.8	75.3±24.1	104.7 ±1.0	81.3±15.7	78.8±19.8	102.0±3.8	103.5 ±0.2
	Walker2D	56.9±25.8	58.3±17.9	57.3±19.9	67.8 ±14.4	85.3±1.3	88.3±1.2	88.8 ±0.9	86.5±0.7
Medium Replay	HalfCheetah	53.5±2.0	56.2±1.5	57.3±1.2	57.5 ±0.9	55.7±0.9	58.9 ±0.7	58.4±0.7	58.9 ±1.3
	Hopper	36.0±2.7	38.1±4.3	42.3±8.4	102.0 ±1.2	69.0±27.0	100.3±3.6	102.9 ±0.5	86.2±20.9
	Walker2D	88.2 ±5.4	75.8±13.6	77.9±13.3	84.8±2.5	83.1±5.0	84.1 ±1.4	82.4±2.9	76.8±0.6
Medium Expert	HalfCheetah	98.0 ±3.6	68.6±17.7	86.9±17.4	74.3±16.8	95.0±1.7	99.5 ±2.4	99.5 ±1.9	99.1±2.5
	Hopper	47.6±8.3	56.3±14.9	65.6±16.1	107.0 ±1.2	104.5±7.7	106.9 ±3.0	102.1±12.6	93.8±10.4
	Walker2D	106.2±1.2	65.9±35.6	83.9±21.3	106.8 ±5.1	107.7±0.8	108.4 ±0.5	107.9±0.4	93.7±25.6
Average		52.1	48.8	55.8	70.4	66.8	70.7	72.7	70.2
IQM		47.9	51.8	59.4	74.4	72.5	78.3	82.5	77.1